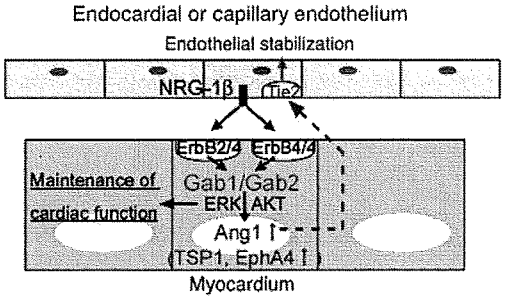

Figure 9
Schematic illustration of the roles of Gab family proteins in the myocardium. NRG-1β shed from the endocardial or capillary endothelium in the heart activates ErbB receptors on the myocardium, resulting in tyrosine phosphorylation of Gab family proteins and subsequent activation of ERK and AKT. NRG-1β/ErbB–Gab1/Gab2 signaling in the myocardium is directly required for postnatal maintenance of myocardial function. In addition, NRG-1β/ErbB–Gab1/Gab2 signaling indirectly contributes to postnatal stabilization of capillary or endocardial endothelium, possibly through Ang1 upregulation (dotted line).

were maintained on a 129/Sv-CS7BL/6J mixed background. We housed all animals in a virus-free facility on a 12-hour light/12-hour dark cycle and fed them a standard mouse food. Animal experiments were approved by the National Cardiovascular Center Research Committee and were performed according to the institutional guidelines.

Histological analyses. Hearts from mice at indicated ages (see Results and Figure 3 legend) were fixed with 10% neutralized formalin, embedded in paraffin, and sectioned at 4 μm thickness. Masson trichrome and elastica van Gieson staining were performed on serial sections. To examine the capillary density, hearts of 4- to 6-week-old mice were fixed with 4% paraformaldehyde, cryoprotected with 20% sucrose, and frozen in OCT compound (Sakura). Cryosections (10 μm) were stained with rat monoclonal anti-CD31 Ab and FITC-conjugated secondary Ab. Paraffin sections of hearts from 4- to 6-week-old mice were immunostained with anti-vWF or anti-α-SMA Ab from the EnVision+ Kit (Dako) according to the manufacturer's instructions.

Physiological analyses. For echocardiography, male mice at the indicated ages were anesthetized with 2.5% avertin (Wako; 15 μl/g body weight). Echocardiography was performed using a Hewlett Packard Sonos 5500 Echocardiography System and a 15-MHz linear transducer. Ventricular dimensions were measured on M-mode images at least 3 times for each group of mice. For hemodynamic measurements, 12-week-old male mice were anesthetized with i.p. injection of urethane (750 mg/kg) and α-chloralose (50 mg/kg) dissolved in normal saline (52). The right common carotid artery was exposed via the midline incision. To allow the use of a physiologic closed-chest preparation, the LV was catheterized retrogradely from the carotid artery using a high-fidelity pressure transducer catheter (1.4 French; Millar Instruments) (53). The LV pressure was digitized, stored on the hard disk of a dedicated laboratory computer system, and analyzed with custom software.

Northern blot analysis. The probes for ANP, α-SKA, and GAPDH were kindly donated by K.R. Chien (Massachusetts General Hospital, Boston, Massachusetts, USA). Total RNA was prepared by TRIzol reagent (Invitrogen) according to the manufacturer's instructions. RNAs from the ventricles of mouse hearts and cultured cardiomyocytes were subjected to Northern blot analyses against a panel of cDNA probes indicated in Results and the legends for Figures 6 and 8. Hybridization was performed using Quikhyb (Stratagene). Quantitative data were collected after normalizing the results to GAPDH.

Gene expression profiling using Affymetrix DNA microarrays. Gene expression in cardiac ventricular tissue was analyzed by Affymetrix microarray hybridization. Control and DKO male mice at 6 weeks of age were injected with 5 μg of NRG-1β or vehicle (normal saline) via tail vein. The ventricles were isolated at 8 hours after injection and subjected to extraction of total RNA using TRIzol reagent. We pooled total RNA from 3 mouse ventricles for each group and subjected to the microarray hybridization as described previously (54). Preparation of cRNA and hybridization of probe on arrays were performed according to the manufacturer's instructions (Affymetrix). Each array experiment was performed in duplicate. FileMaker Pro 8.0 software was used to analyze genes that demonstrated identical patterns in 2 independent microarray experiments. Data were analyzed according to the minimum information about a microarray experiment (MIAME) rule. Annotation of the probe numbers and targeted sequences are shown on the Affymetrix website (https://www.affymetrix.com/site/login/login.affx).

Statistics. All data are expressed as mean ± SEM. Differences among multiple groups were compared by 1-way ANOVA followed by a post-hoc comparison using Scheffe's method. The 2-tailed Student's *t* test was used to analyze differences between 2 groups. $P < 0.05$ was considered statistically significant. Survival curves were generated using Kaplan-Meier method, and significance was evaluated using the log-rank test.

Acknowledgments

This work was supported in part by grants from the Ministry of Education, Culture, Sports, Science, and Technology of Japan (to Y. Nakaoka and N. Mochizuki); the Ministry of Health, Labour, and Welfare of Japan (to N. Mochizuki); the Program for the Promotion of Fundamental Studies in Health Sciences of the National Institute of Biomedical Innovation (to T. Minami, T. Kodama, and N. Mochizuki); the Japan Heart Foundation (Novartis Grant for Research Award on Molecular and Cellular Cardiology, to Y. Nakaoka); the Mitsubishi Pharma Research Foundation (to Y. Nakaoka); and the Uehara Memorial Foundation (to Y. Nakaoka). We thank Y. Matsuura, M. Yoshida, M. Miyabayashi, M. Maeoka, Y. Ohba, M. Sato, K. Sako, and K. Shioya for their technical assistance; S. Higashiyama, O. Nakagawa, and O. Ohara for helpful comments; K. Komamura for advice on echocardiography; and W.W. Hall and K. Yamauchi-Takihara for critical reading of the manuscript.

Received for publication October 16, 2006, and accepted in revised form April 10, 2007.

Address correspondence to: Naoki Mochizuki, Department of Structural Analysis, National Cardiovascular Center Research Institute, 5-7-1 Fujishirodai, Suita, Osaka 565-8565, Japan. Phone: 81-6-6833-5012, ext. 2508; Fax: 81-6-6835-5461; E-mail: nmochizu@ri.ncvc.go.jp. Or to: Yoshikazu Nakaoka: Department of Cardiovascular Medicine, Osaka University Graduate School of Medicine, 2-2, Yamada-oka, Suita, Osaka 565-0871, Japan. Phone: 81-6-6879-3835; Fax: 81-6-6879-3839; E-mail: ynakaoka@imed3.med.osaka-u.ac.jp.

Y. Nakaoka's present address is: Department of Cardiovascular Medicine, Osaka University Graduate School of Medicine, Osaka, Japan.

Hisao Hirota is deceased.

1. Seidman, J.G., and Seidman, C. 2001. The genetic basis for cardiomyopathy: from mutation identification to mechanistic paradigms. *Cell.* **104**:557–567.
2. Chien, K.R. 1999. Stress pathways and heart failure. *Cell.* **98**:555–558.
3. Schlessinger, J., and Lemmon, M.A. 2003. SH2 and PTB domains in tyrosine kinase signaling. *Sci. STKE.* **2003**:RE12.
4. Gu, H., and Neel, B.G. 2003. The "Gab" in signal transduction. *Trends Cell Biol.* **13**:122–130.
5. Nishida, K., and Hirano, T. 2003. The role of Gab family scaffolding adapter proteins in the signal transduction of cytokine and growth factor receptors. *Cancer Sci.* **94**:1029–1033.
6. Itoh, M., et al. 2000. Role of Gab1 in heart, placenta, and skin development and growth factor- and cytokine-induced extracellular signal-regulated kinase mitogen-activated protein kinase activation. *Mol. Cell. Biol.* **20**:3695–3704.
7. Sachs, M., et al. 2000. Essential role of Gab1 for signaling by the c-Met receptor in vivo. *J. Cell Biol.* **150**:1375–1384.
8. Gu, H., et al. 2001. Essential role for Gab2 in the allergic response. *Nature.* **412**:186–190.
9. Nishida, K., et al. 2002. Requirement of Gab2 for mast cell development and KitL/c-Kit signaling. *Blood.* **99**:1866–1869.
10. Wada, T., et al. 2005. The molecular scaffold Gab2 is a crucial component of RANK signaling and osteoclastogenesis. *Nat. Med.* **11**:394–399.
11. Nishida, K., et al. 2005. FcepsilonRI-mediated mast cell degranulation requires calcium-independent microtubule-dependent translocation of granules to the plasma membrane. *J. Cell Biol.* **170**:115–126.
12. Seiffert, M., et al. 2003. Gab3-deficient mice exhibit normal development and hematopoiesis and are immunocompetent. *Mol. Cell. Biol.* **23**:2415–2424.
13. Nakaoka, Y., et al. 2003. Activation of gp130 transduces hypertrophic signal through interaction of scaffolding/docking protein Gab1 with tyrosine phosphatase SHP2 in cardiomyocytes. *Circ. Res.* **93**:221–229.
14. Bentires-Alj, M., et al. 2006. A role for the scaffolding adapter GAB2 in breast cancer. *Nat. Med.* **12**:114–121.
15. Yamasaki, S., et al. 2003. Gab1 is required for EGF receptor signaling and the transformation by activated ErbB2. *Oncogene.* **22**:1546–1556.
16. Brutsaert, D.L. 2003. Cardiac endothelial-myocardial signaling: its role in cardiac growth, contractile performance, and rhythmicity. *Physiol. Rev.* **83**:59–115.
17. Garratt, A.N., Ozcelik, C., and Birchmeier, C. 2003. ErbB2 pathways in heart and neural diseases. *Trends Cardiovasc. Med.* **13**:80–86.
18. Falls, D.L. 2003. Neuregulins: functions, forms, and signaling strategies. *Exp. Cell Res.* **284**:14–30.
19. Iwamoto, R., and Mekada, E. 2006. ErbB and HB-EGF signaling in heart development and function. *Cell Struct. Funct.* **31**:1–14.
20. Lemmens, K., Segers, V.F., Demolder, M., and De Keulenaer, G.W. 2006. Role of neuregulin-1/ErbB2 signaling in endothelium-cardiomyocyte crosstalk. *J. Biol. Chem.* **281**:19469–19477.
21. Zhao, Y.Y., et al. 1998. Neuregulins promote survival and growth of cardiac myocytes. Persistence of ErbB2 and ErbB4 expression in neonatal and adult ventricular myocytes. *J. Biol. Chem.* **273**:10261–10269.
22. Gassmann, M., et al. 1995. Aberrant neural and cardiac development in mice lacking the ErbB4 neuregulin receptor. *Nature.* **378**:390–394.
23. Lee, K.F., et al. 1995. Requirement for neuregulin receptor erbB2 in neural and cardiac development. *Nature.* **378**:394–398.
24. Meyer, D., and Birchmeier, C. 1995. Multiple essential functions of neuregulin in development. *Nature.* **378**:386–390.
25. Iwamoto, R., et al. 2003. Heparin-binding EGF-like growth factor and ErbB signaling is essential for heart function. *Proc. Natl. Acad. Sci. U. S. A.* **100**:3221–3226.
26. Jackson, L.F., et al. 2003. Defective valvulogenesis in HB-EGF and TACE-null mice is associated with aberrant BMP signaling. *EMBO J.* **22**:2704–2716.
27. Slamon, D.J., et al. 2001. Use of chemotherapy plus a monoclonal antibody against HER2 for metastatic breast cancer that overexpresses HER2. *N. Engl. J. Med.* **344**:783–792.
28. Suter, T.M., Cook-Bruns, N., and Barton, C. 2004. Cardiotoxicity associated with trastuzumab (Herceptin) therapy in the treatment of metastatic breast cancer. *Breast.* **13**:173–183.
29. Crone, S.A., et al. 2002. ErbB2 is essential in the prevention of dilated cardiomyopathy. *Nat. Med.* **8**:459–465.
30. Garcia-Rivello, H., et al. 2005. Dilated cardiomyopathy in Erb-b4-deficient ventricular muscle. *Am. J. Physiol. Heart Circ. Physiol.* **289**:H1153–H1160.
31. Ozcelik, C., et al. 2002. Conditional mutation of the ErbB2 (HER2) receptor in cardiomyocytes leads to dilated cardiomyopathy. *Proc. Natl. Acad. Sci. U. S. A.* **99**:8880–8885.
32. Nakagawa, O., et al. 1995. Rapid transcriptional activation and early mRNA turnover of brain natriuretic peptide in cardiocyte hypertrophy. Evidence for brain natriuretic peptide as an "emergency" cardiac hormone against ventricular overload. *J. Clin. Invest.* **96**:1280–1287.
33. Cote, G.M., Miller, T.A., Lebrasseur, N.K., Kuramochi, Y., and Sawyer, D.B. 2005. Neuregulin-1alpha and beta isoform expression in cardiac microvascular endothelial cells and function in cardiac myocytes in vitro. *Exp. Cell Res.* **311**:135–146.
34. Agah, R., et al. 1997. Gene recombination in postmitotic cells. Targeted expression of Cre recombinase provokes cardiac-restricted, site-specific rearrangement in adult ventricular muscle in vivo. *J. Clin. Invest.* **100**:169–179.
35. Yamaguchi, O., et al. 2004. Cardiac-specific disruption of the c-raf-1 gene induces cardiac dysfunction and apoptosis. *J. Clin. Invest.* **114**:937–943. doi:10.1172/JCI200420317.
36. Meng, S., Chen, Z., Munoz-Antonia, T., and Wu, J. 2005. Participation of both Gab1 and Gab2 in the activation of the ERK/MAPK pathway by epidermal growth factor. *Biochem. J.* **391**:143–151.
37. Moss, A.J., and Adams, F.H. 1995. *Moss' heart disease in infants, children, and adolescents.* Williams & Wilkins. Baltimore, Maryland, USA. 1,085 pp.
38. Westwood, M., Harris, R., Burn, J.L., and Barson, A.J. 1975. Heredity in primary endocardial fibroelastosis. *Br. Heart J.* **37**:1077–1084.
39. Xu, X., et al. 2005. ASF/SF2-regulated CaMKIIdelta alternative splicing temporally reprograms excitation-contraction coupling in cardiac muscle. *Cell.* **120**:59–72.
40. Brindle, N.P., Saharinen, P., and Alitalo, K. 2006. Signaling and functions of angiopoietin-1 in vascular protection. *Circ. Res.* **98**:1014–1023.
41. Davis, S., et al. 1996. Isolation of angiopoietin-1, a ligand for the TIE2 receptor, by secretion-trap expression cloning. *Cell.* **87**:1161–1169.
42. Suri, C., et al. 1996. Requisite role of angiopoietin-1, a ligand for the TIE2 receptor, during embryonic angiogenesis. *Cell.* **87**:1171–1180.
43. Baliga, R.R., et al. 1999. NRG-1-induced cardiomyocyte hypertrophy. Role of PI-3-kinase, p70(S6K), and MEK-MAPK-RSK. *Am. J. Physiol.* **277**:H2026–H2037.
44. Lawler, J. 2000. The functions of thrombospondin-1 and-2. *Curr. Opin. Cell Biol.* **12**:634–640.
45. Ogita, H., et al. 2003. EphA4-mediated Rho activation via Vsm-RhoGEF expressed specifically in vascular smooth muscle cells. *Circ. Res.* **93**:23–31.
46. Liao, W., et al. 1997. The zebrafish gene cloche acts upstream of a flk-1 homologue to regulate endothelial cell differentiation. *Development.* **124**:381–389.
47. Nebigil, C.G., et al. 2000. Serotonin 2B receptor is required for heart development. *Proc. Natl. Acad. Sci. U. S. A.* **97**:9508–9513.
48. Sato, T.N., et al. 1995. Distinct roles of the receptor tyrosine kinases Tie-1 and Tie-2 in blood vessel formation. *Nature.* **376**:70–74.
49. Nishida, K., et al. 1999. Gab-family adapter proteins act downstream of cytokine and growth factor receptors and T- and B-cell antigen receptors. *Blood.* **93**:1809–1816.
50. Osugi, T., et al. 2002. Cardiac-specific activation of signal transducer and activator of transcription 3 promotes vascular formation in the heart. *J. Biol. Chem.* **277**:6676–6681.
51. Taniguchi, M., et al. 1998. Efficient production of Cre-mediated site-directed recombinants through the utilization of the puromycin resistance gene, pac: a transient gene-integration marker for ES cells. *Nucleic Acids Res.* **26**:679–680.
52. Georgakopoulos, D., et al. 1998. In vivo murine left ventricular pressure-volume relations by miniaturized conductance micromanometry. *Am. J. Physiol.* **274**:H1416–H1422.
53. Nishio, R., Sasayama, S., and Matsumori, A. 2002. Left ventricular pressure-volume relationship in a murine model of congestive heart failure due to acute viral myocarditis. *J. Am. Coll. Cardiol.* **40**:1506–1514.
54. Minami, T., Miura, M., Aird, W.C., and Kodama, T. 2006. Thrombin-induced autoinhibitory factor, Down syndrome critical region-1, attenuates NFAT-dependent vascular cell adhesion molecule-1 expression and inflammation in the endothelium. *J. Biol. Chem.* **281**:20503–20520.

Molecular Biology of the Cell
Vol. 18, 1850–1860, May 2007

R-Ras Regulates Exocytosis by Rgl2/Rlf-mediated Activation of RalA on Endosomes[D] [V]

Akiyuki Takaya,*† Takahiro Kamio,* Michitaka Masuda,‡ Naoki Mochizuki,‡ Hirofumi Sawa,§ Mami Sato,§ Kazuo Nagashima,§ Akiko Mizutani,‖ Akira Matsuno,¶ Etsuko Kiyokawa,† and Michiyuki Matsuda*†

*Department of Signal Transduction, Research Institute for Microbial Diseases, Osaka University, Yamadaoka, Osaka 565-0871, Japan; †Department of Pathology and Biology of Diseases, Graduate School of Medicine, Kyoto University, Kyoto 606-8501, Japan; ‡Department of Structural Analysis, National Cardiovascular Center Research Institute, Osaka 565-8565, Japan; §Laboratory of Molecular and Cellular Pathology, Graduate School of Medicine, Hokkaido University, Sapporo 060-8638, Japan; ‖Basic Medical Science and Molecular Medicine, Tokai University School of Medicine, Kanagawa 259-1193, Japan; and ¶Department of Neurosurgery, Teikyo University Ichihara Hospital, Chiba 299-0111, Japan

Submitted August 29, 2006; Revised February 16, 2007; Accepted February 28, 2007
Monitoring Editor: Mark Ginsberg

R-Ras is a Ras-family small GTPase that regulates various cellular functions such as apoptosis and cell adhesion. Here, we demonstrate a role of R-Ras in exocytosis. By the use of specific anti-R-Ras antibody, we found that R-Ras was enriched on both early and recycling endosomes in a wide range of cell lines. Using a fluorescence resonance energy transfer-based probe for R-Ras activity, R-Ras activity was found to be higher on endosomes than on the plasma membrane. This high R-Ras activity on the endosomes correlated with the accumulation of an R-Ras effector, the Rgl2/Rlf guanine nucleotide exchange factor for RalA, and also with high RalA activity. The essential role played by R-Ras in inducing high levels of RalA activity on the endosomes was evidenced by the short hairpin RNA (shRNA)-mediated suppression of R-Ras and by the expression of R-Ras GAP. In agreement with the reported role of RalA in exocytosis, the shRNA of either R-Ras or RalA was found to suppress calcium-triggered exocytosis in PC12 pheochromocytoma cells. These data revealed that R-Ras activates RalA on endosomes and that it thereby positively regulates exocytosis.

INTRODUCTION

R-Ras is a Ras-family GTPase and its amino acid sequence is 55% identical to those of the classical types of Ras (H-, K-, N-Ras, collectively referred to hereafter as "Ras") (Lowe *et al.*, 1987). As is the case with the other Ras-family GTPases, R-Ras is regulated primarily by two classes of protein, guanine nucleotide exchange factor (GEF) and GTPase-activating protein (GAP). Reflecting the high sequence similarity among Ras-family GTPases, many GEFs and GAPs for R-Ras catalyze other Ras-family GTPases as well (Ohba *et al.*, 2000). Furthermore, R-Ras is known to interact with many effectors of Ras, such as Raf-1, Ral GEFs, and the p110α subunit of phosphoinositide 3-kinase (PI3K) (Rey *et al.*, 1994; Spaargaren and Bischoff, 1994; Spaargaren *et al.*, 1994; Marte *et al.*, 1997). Despite this redundancy between R-Ras and Ras, R-Ras exhibits various properties that are distinct from those of Ras. For example, R-Ras preferentially activates Ral GEFs and PI3K, but it does not activate Raf (Huff *et al.*, 1997; Rodriguez-Viciana *et al.*, 2004). The transforming activity of constitutively active R-Ras is substantially less potent than that of the constitutively active Ras (Cox *et al.*, 1994), although it should be noted that a recent report has suggested the involvement of R-Ras in human gastric cancer (Nishigaki *et al.*, 2005). Meanwhile, R-Ras is known to regulate cell adhesion, cell spreading, and phagocytosis through the activation of integrin (Zhang *et al.*, 1996; Keely *et al.*, 1999; Berrier *et al.*, 2000; Self *et al.*, 2001). R-Ras-null mice have recently been shown to exhibit excessive vascular responses, in spite of the fact that they are otherwise normal (Komatsu and Ruoslahti, 2005). This phenotype seems to reflect higher levels of expression of R-Ras in smooth muscle cells, including blood vessel cells. The results obtained with R-Ras-null mice have also demonstrated that an R-Ras defect can be almost entirely compensated for by other gene products.

Ral GEFs, effectors of Ras-family GTPases, are activators of the two Ral proteins, RalA and RalB, which are also Ras-family GTPases (Wolthuis and Bos, 1999; Quilliam *et al.*, 2002; Rodriguez-Viciana *et al.*, 2004). It has been suggested that this Ral GEFs-Ral pathway is more important in the Ras-dependent oncogenesis of human cells than are other Ras-dependent pathways, such as those involving Raf and PI3K (Hamad *et al.*, 2002; Rangarajan *et al.*, 2004; Lim *et al.*, 2005; Gonzalez-Garcia *et al.*, 2005). The activated Ral then binds to various Ral-binding proteins and thereby regulates

This article was published online ahead of print in *MBC in Press* (http://www.molbiolcell.org/cgi/doi/10.1091/mbc.E06-08-0765) on March 7, 2007.

[D] [V] The online version of this article contains supplemental material at *MBC Online* (http://www.molbiolcell.org).

Address correspondence to: Michiyuki Matsuda (matsudam@path1.kyoto-u.ac.jp).

Abbreviations used: EGF, epidermal growth factor; FRET, fluorescence (Förster's) resonance energy transfer; GAP, GTPase-activating protein; GEF, guanine nucleotide exchange factor; NPY, neuropeptide Y; PI3K, p110α subunit of phosphoinositide-3-kinase.

various cellular functions (Feig, 2003). The characterization of such Ral effector proteins has suggested that Ral may be involved in vesicular trafficking. For example, the Ral-binding protein RalBP1 is thought to regulate endocytosis, suggesting the involvement of Ral in endocytosis (Nakashima *et al.*, 1999). Ral may also regulate exocytosis, because Ral binds to two components of the exocyst complex, Sec5 and Exo84 (Moskalenko *et al.*, 2002, 2003).

The exocyst complex was originally identified by genetic and biochemical studies as a cluster of molecules required for exocytosis in budding yeast, and it was later characterized in a wide range of eukaryotes. The exocyst complex consists of eight subunits: Sec3, Sec5, Sec6, Sec8, Sec10, Sec15, Exo70, and Exo84 (Lipschutz and Mostov, 2002). These proteins are primarily involved in the tethering and/or docking process of trafficking vesicles, which occurs before the fusion process (Finger *et al.*, 1998; Tsuboi *et al.*, 2005). Due to their fundamental role in exocytosis, any malfunction of the proteins in the exocyst complex can disrupt various cellular events, such as the basolateral transport of vesicles in polarized epithelial cells, neurite outgrowth in PC12 cells, paraxial mesoderm formation in mice, and secretory vesicle-mediated abscission in *Drosophila* (Friedrich *et al.*, 1997; Grindstaff *et al.*, 1998; Vega and Hsu, 2001; Murthy *et al.*, 2003; Gromley *et al.*, 2005).

To gain a better understanding of the function of R-Ras and its potential role in Ral-mediated exocytosis, it will be essential to elucidate not only the subcellular localization but also the activity change of these proteins. Thus, we developed specific anti-R-Ras sera and a probe for R-Ras activity based on the principle of fluorescence resonance energy transfer (FRET), a technique that has been shown to be extremely useful for the spatiotemporal analysis of small GTPases (Kurokawa *et al.*, 2004b). Using these tools, we found that endogenous R-Ras is enriched and activated at endosomes and that these R-Ras proteins promote exocytosis by activating RalA.

MATERIALS AND METHODS

Probes Based on FRET

FRET probes for R-Ras, designated as Raichu-R-Ras, were prepared essentially as described previously (Mochizuki *et al.*, 2001; Takaya *et al.*, 2004). From the amino terminus, Raichu-R-Ras consisted of a modified yellow fluorescent protein (YFP) designated as "Venus" (Nagai *et al.*, 2002) (amino acids [aa] 1-239), a spacer (Leu-Asp), human R-Ras (aa 1-199), a 17-amino acid-spacer (Gly-Gly-Gly-Thr-Gly-Gly-Gly-Gly-Ser-Gly-Gly-Thr-Gly-Gly-Gly-Thr), the Ras-binding domain of RalGDS (aa 785-871), a spacer (Gly-Gly-Arg), a modified cyan fluorescent protein (CFP) designated as "SECFP" ($Lys^{27}Arg$, $Asp^{130}Ala$, $Asn^{165}His$, $Ser^{176}Gly$) (aa 1-237), a spacer (Gly-Arg-Ser-Arg), and the carboxy-terminal region of R-Ras (aa 195-218) (Figure 1A). The characterization of Raichu R-Ras was performed as described previously (Takaya *et al.*, 2004).

Plasmids

pCXN2-mCFP, pCXN2-mRFP, and pCXN2-mCherry are expression vectors encoding a monomeric SECFP (Zacharias *et al.*, 2002), a monomeric red fluorescent protein (RFP) (Kurokawa *et al.*, 2004a), and mCherry, respectively. cDNA of mCherry was provided by R. Y. Tsien (University of California at San Diego). The pERedNLS and pERedMito expression vectors contain an internal ribosomal site followed by the cDNAs of DsRed-Express (Clontech, Mountain View, CA) with nuclear and mitochondrial localization signals, respectively (Aoki *et al.*, 2005). pCXN2-5Myc and pCXN2-Flag are mammalian expression vectors containing Myc and Flag epitope tags, respectively. cDNAs of RalBP1 and Rgl were provided by A. Kikuchi (Hiroshima University, Hiroshima, Japan). cDNA of p110α and p85α were obtained from Y. Fukui (University of Tokyo, Tokyo, Japan), and cDNA of Rab5A was obtained from Y. Takai (Osaka University, Osaka, Japan). Rap1B cDNA was provided by N. Minato (Kyoto University, Kyoto, Japan). The cDNAs of K-Ras and N-Ras were obtained from L. A. Feig (Tufts University, Boston, MA). cDNAs of Rab7, Rab11A, and RalB were purchased from Guthrie cDNA Resource Center (Sayre, PA). pAcGFP1-Endo was purchased from Clontech. pVenus-N1-NPY was obtained from A. Miyawaki (The Brain Science Institute, RIKEN, Wako-shi, Japan) (Nagai *et al.*, 2002). pHA-EYFP-GH1 has been described previously (Matsuno *et al.*, 2005). pCXN2-Flag-CalDAG-GEFII, pCXN2-Flag-CalDAG-GEFIII, pCXN2-Flag-R-RasGAP, pCAGGS-Flag-p120RasGAP, pCXN2-Flag-rap1GAP1B, pCAGGS-RasGRF, pCAGGS-mSos1, and pEF-BOS-myc-$Gap1^m$ have been described previously (Yamamoto *et al.*, 1995; Gotoh *et al.*, 1997; Ohba *et al.*, 2000). pCXN2-5Myc-R-Ras-rRNAi (RNA interference-resistant clone) encodes a R-Ras mutant resistant to the short hairpin RNA (shRNA) vector. For the preparation of the glutathione S-transferase (GST) fusion proteins, cDNAs were subcloned into pGEX vectors and recombinant proteins were prepared according to the manufacturer's protocol (GE Healthcare, Little Chalfont, Buckinghamshire, United Kingdom).

Cells, Antibodies, and Reagents

293T cells were obtained from B. J. Mayer (University of Connecticut, Storrs, CT). The line of Cos7 cells used in this study was Cos7/E3, a subclone of Cos7 cells established by Y. Fukui. The PC12 cells were obtained from S. Kuroda (University of Tokyo). HeLa and Madin-Darby canine kidney (MDCK) cells were purchased from the Human Science Research Resources Bank (Sennan-shi, Osaka, Japan). The GH3 cells used here have been described previously (Matsuno *et al.*, 2005). The PC12 cells were maintained in DMEM (Sigma-Aldrich, St. Louis, MO) supplemented with 10% fetal calf serum and 5% horse serum. GH3 cells were cultured in Ham's F-10 (Sigma-Aldrich) supplemented with 15% horse serum and 2.5% fetal calf serum. Other cells were maintained in DMEM supplemented with 10% fetal calf serum. GH3 cells stably expressing R-Ras were prepared essentially as described previously (Akagi *et al.*, 2003). Anti-green fluorescent protein (GFP) rabbit serum was prepared in our laboratory. Anti-RalA and anti-RalB were purchased from BD Biosciences (San Jose, CA). Anti-FLAG M2 and tetradecanoyl phorbol-13-acetate (TPA) was purchased from Sigma-Aldrich. Anti-Myc 9E10 was obtained from Santa Cruz Biotechnology (Santa Cruz, CA). Anti-GFP antibody was also purchased from Takara Bio (Otsu, Japan). Anti-Akt, anti-phospho Akt (Thr308), anti-phospho-mitogen-activated protein kinase kinase (MEK) 1/2 (Ser217/221), and anti-R-Ras were purchased from Cell Signaling Technology (Beverly, MA). Alexa 488 anti-rabbit immunoglobulin G (IgG), Alexa 488 anti-rat IgG, and Alexa 568 anti-mouse IgG were purchased from Invitrogen (San Diego, CA). To generate anti-R-Ras sera, three rabbits were injected with GST-R-Ras.

RNA Interference

Synthetic siRNAs against R-Ras and Ral proteins were prepared as described previously (Oinuma *et al.*, 2004; Wozniak *et al.*, 2005). siRNAs were transfected using Oligofectamine or Lipofectamine 2000 (Invitrogen) according to the manufacturer's instructions. pSuper.retro.puro vector (OligoEngine, Seattle, WA) was used for short hairpin RNA. The shRNA sequences for rat R-Ras and RalA have been described previously (Oinuma *et al.*, 2004; Vitale *et al.*, 2005), and the sequence for rat RalB was 5'-GCCGACAGTTACAGAAAGA-3'. After transfection, the cells were incubated for at least 48 h before analysis.

Bos' Pull-Down Assay

Bos' pull-down assay for Ral proteins was performed essentially as described previously (Takaya *et al.*, 2004). Briefly, the cells were lysed in Ral buffer (50 mM Tris-HCl, pH 7.5, 200 mM NaCl, 2.5 mM $MgCl_2$, 1% NP-40, 10% glycerol, 1 mM Na_3VO_4, 1 mM phenylmethylsulfunyl fluoride, 10 μg/ml aprotinin, and 10 μg/ml leupeptin) and were clarified by centrifugation. The supernatant was incubated with GST-Sec5-RBD or GST-RalBP1-RBD for 30 min at 4°C. The resulting complexes of Ral-GTP and GST fusion proteins were incubated with glutathione-Sepharose beads (GE Healthcare) for 1 h at 4°C, and after the bound proteins and cell lysates had been separated by SDS-polyacrylamide gel electrophoresis (PAGE), immunoblotting with anti-RalA or anti-RalB antibody was carried out. Bound antibodies were detected by an ECL chemiluminescence detection system (GE Healthcare), and binding was quantified with the aid of an LAS-1000 image analyzer (Fuji-Film, Tokyo, Japan). The pull-down assay for Ras, Rap1, and R-Ras was performed essentially as described above except for the use of GST-RalGDS-RBD.

Immunoprecipitation

Transfected Cos7 cells were harvested in ice-cold lysis buffer (50 mM Tris-HCl pH 7.5, 200 mM NaCl, 2.5 mM $MgCl_2$, 1% NP-40, 0.5% sodium deoxycholate, 10% glycerol, 1 mM Na_3VO_4, 1 mM phenylmethylsulfunyl fluoride, 10 μg/ml aprotinin, and 10 μg/ml leupeptin). Anti-Myc antibody, GFP antiserum, or R-Ras antiserum was added to the cleared lysates. After the lysates were subjected to 1 h of rotation at 4°C with protein G-Sepharose or protein A-Sepharose (GE Healthcare), the beads were washed and boiled in sample buffer. The bound proteins were then subjected to immunoblot analysis.

Immunohistochemistry and Immunogold Electron Microscopy

Formalin-fixed, paraffin-embedded sections were deparaffinized with xylenes and rehydrated with ethanol. The sections were treated with normal goat serum and 1% H_2O_2 to quench endogenous peroxidase activity, and then they

were incubated with primary antibody overnight at 4°C. After incubation of the sections with the biotinylated secondary antibody, immunopositive signals were visualized using 3,3'-diaminobenzidine tetrahydrochloride as a chromogen. For immunogold electron microscopy, the cells were fixed with 4% paraformaldehyde, 0.35% glutaraldehyde, and 0.2% picric acid at 4°C for 1.5 h, followed by fixation with 4% paraformaldehyde and 0.2% picric acid overnight at 4°C. After being washed with phosphate-buffered saline (PBS), the cells were dehydrated with ethanol and embedded in Lowicryl K4M (Polysciences; Tokyo, Japan). Ultrathin sections were placed on nickel grids and were immersed in a target retrieval solution (Dako Denmark, Glostrup, Denmark). Then, the samples were exposed to microwave radiation for 20 min, after which they were washed with distilled water. The grids were incubated with anti-R-Ras or preimmune rabbit serum at room temperature for 2 h, and then they were incubated for 1 h with anti-rabbit IgG labeled with 10-nm gold particles (GE Healthcare). After being washed and dried, the sections were stained with both uranyl acetate and lead citrate; the sections were then examined with a Hitachi H-800 transmission electron microscope (Hitachi High-Technologies, Tokyo, Japan). In some experiments, MDCK cells expressing an endosomal marker protein, AcGFP-Endo, were used for the analysis. Cells were double stained with anti-R-Ras rabbit serum and anti-GFP mouse monoclonal antibody (mAb) JL-8, which were detected with anti-rabbit IgG labeled with 5-nm gold particles and anti-mouse IgG labeled with 10-nm gold particles, respectively. As a control, anti-R-Ras rabbit serum preadsorbed to GST-R-Ras, preimmune rabbit serum, nonspecific rabbit IgG, or nonspecific mouse IgG was also used.

Immunocytochemistry

To stain the endogenous R-Ras protein, MDCK cells were fixed with 3.7% formaldehyde and then subjected to refixation with methanol at −20°C and permeabilization with 0.2% Triton X-100, followed by incubation in PBS containing 3% bovine serum albumin (BSA) and 0.02% Triton X-100 for 1 h. In some experiments, MDCK cells were fixed with 4% paraformaldehyde, immediately followed by permeabilization with 0.01% Triton X-100 for 1 min and incubation with 2% BSA in 50 mM NH_4Cl-containing PBS. These fixed cells were incubated for 1 h at room temperature with anti R-Ras rabbit serum, washed with PBS, and then incubated for 30 min at room temperature with Alexa 488 anti-rabbit IgG. For the 3HA-tag and 5Myc-tag staining, Cos7 cells were fixed with 3% paraformaldehyde and subjected to permeabilization and staining as described above. Alexa 488 anti-rat IgG and Alexa 568 anti-mouse IgG were used to detect anti-hemagglutinin (HA) and anti-Myc, respectively. After being washed, the cells were imaged with an FV-500 confocal microscope equipped with an argon laser and with an HeNe laser microscope (Olympus, Tokyo, Japan). Twenty-five XY images scanned from the bottom to the top of the cells were obtained to prepare stacked images of XY and XZ sections.

Imaging of R-Ras and RalA Activity in Living Cells

R-Ras and RalA activity was visualized with Raichu-R-Ras or Raichu-RalA essentially as described previously (Mochizuki *et al.*, 2001; Takaya *et al.*, 2004). Expression plasmids were transfected into Cos7 cells by Polyfect (QIAGEN, Valencia, CA) or 293fectin (Invitrogen). More than 36 h after transfection, the cells were imaged with an Olympus IX70 inverted microscope equipped with an image splitter, Dual-View (Optical Insights, Santa Fe, NM) and an EMCCD camera, iXon DV887 (Andor Technology, Belfast, United Kingdom), and the imaging process was controlled by MetaMorph software (Molecular Devices, Sunnyvale, CA). In some experiments, cells were imaged with an Olympus IX81 inverted microscope equipped with a laser-based autofocusing system, IX2-ZDC, and an automatically programmable XY stage, MD-XY30100T-Meta, which allowed us to obtain the time-lapse images of several view fields in a single experiment. For dual-emission ratio imaging of the Raichu probes, we used previously described filter sets (Takaya *et al.*, 2004), and we obtained images for CFP and FRET. After background subtraction was carried out, the FRET/CFP ratio was depicted using MetaMorph software, and this image was used to represent FRET efficiency. Confocal FRET images were obtained by an IX51 upright fluorescence microscope (Olympus) equipped with a CSU-10 spinning Nipkow disk confocal unit (Yokogawa, Tokyo, Japan), a W-view (Hamamatsu Photonics, Hamamatsu, Japan), and a diode-pumped solid state 430-nm laser (Melles Griot, Carlsbad, CA).

Exocytosis Assay

The exocytosis assay was carried out using Venus-tagged neuropeptide Y (NPY) as described previously (Nagai *et al.*, 2002). pVenus-N1-NPY or pHA-EYFP-GH1 with or without additional expression vectors was transfected into PC12 cells or GH3 cells with Lipofectamine 2000 (Invitrogen). Sixty hours after transfection, the cells were washed in a low-potassium saline solution (145 mM NaCl, 5.6 mM KCl, 2.2 mM $CaCl_2$, 0.5 mM $MgCl_2$, 5.6 mM glucose, and 15 mM HEPES, pH 7.4). Then, the medium was exchanged for a high-potassium saline medium (95 mM NaCl, 56 mM KCl, 2.2 mM $CaCl_2$, 0.5 mM $MgCl_2$, 5.6 mM glucose, and 15 mM HEPES, pH 7.4) to depolarize the cells. After 20 min in the case of the PC12 cells or 10 min in the case of the GH3 cells, cell-free supernatants were collected and were stored as the secreted fraction. Cells remaining on the culture dishes were lysed in PBS containing 1% Triton X-100, and they were cleared by centrifugation to obtain the nonsecreted fraction. The fluorescence of NPY-Venus or EYFP-GH recovered in each fraction was measured by a FluoroSkan II fluorescence microplate reader (Global Medical Instrumentation, Ramsey, MN).

Online Supplemental Material

Time-lapse FRET images of Supplemental Figure S3J and Figure 3B are compiled into QuickTime videos available as supplemental material. Movie 1 shows Cos7 cells transfected with pRaichu-R-Ras and stimulated with TPA as described in the legend to Supplemental Figure S3K. Movie 2 shows Cos7 cells transfected with pRaichu-R-Ras as described in the legend to Figure 2B. Images were acquired every 30 s, and the video is displayed at 15 frames per second. Supplemental Figures 1–6 show characterization of anti-R-Ras serum, images of colocalization studies, basic property of Raichu-R-Ras probe, and results of coimmunoprecipitation studies.

RESULTS

Tissue Distribution of Endogenous R-Ras

One of the reasons why the biological function of R-Ras remains elusive may be the lack of information concerning its tissue distribution and subcellular localization, which in turn is likely due to the lack of a specific antiserum. Therefore, we developed high-affinity anti-R-Ras sera that could be used for immunohistochemistry. One of the antisera was found to specifically recognize the endogenous R-Ras protein by immunoblotting analysis (Supplemental Figure S1). The obtained anti-R-Ras serum was used for immunohistochemical analyses. We found that R-Ras accumulated at high levels in the cytoplasm of smooth muscle cells, including those in the intestine and blood vessels, as has been reported recently (Komatsu and Ruoslahti, 2005) (Figure 1A). To a lesser extent, R-Ras expression was also observed in the neuroendocrine cells of the adrenal medulla and in islet cells in the pancreas (Figure 1B). Immunohistochemistry analysis in other tissues is described in Supplemental Figure S2.

Localization of Endogenous R-Ras on the Vesicular Structures Related to Early and Recycling Endosomes

To more closely analyze the subcellular distribution of R-Ras, we chose MDCK cells, which were found to express R-Ras most abundantly among the cell lines examined (Supplemental Figure S1C). Quantitative immunoblotting analysis revealed that the number of R-Ras molecules was 1.5×10^5/cell, which was about one fifth of the number of Ras molecules but similar to the numbers of RalA and RalB molecules (data not shown). In MDCK cells, endogenous R-Ras was enriched on the vesicles and/or on endosome-like structures, although weak staining of the plasma membrane was also clearly seen (Figure 1, C and D). Such vesicular structures were not observed with preimmune sera or anti-R-Ras serum preabsorbed with antigen (data not shown). To further investigate the nature of R-Ras–positive endosomes, R-Ras was coexpressed with endosomal markers (Figure 2). R-Ras localization was found to overlap significantly with that of transferrin (early and recycling endosomes), Rab4A (early and recycling endosomes), Rab5A (early endosome), and Rab11A (recycling endosome), but not with that of EEA1 (early endosome) and Rab7 (late endosome). Immunoelectron micrographs showed that R-Ras was localized on cytoplasmic vesicular structures that were ~50 nm in diameter (Figure 1E). Furthermore, double staining showed the colocalization of R-Ras and AcGFP-Endo, an endosomal marker (Figure 1F). These results indicated that the R-Ras–loaded vesicles were related to early and recycling endosomes, but not to the late endosomes.

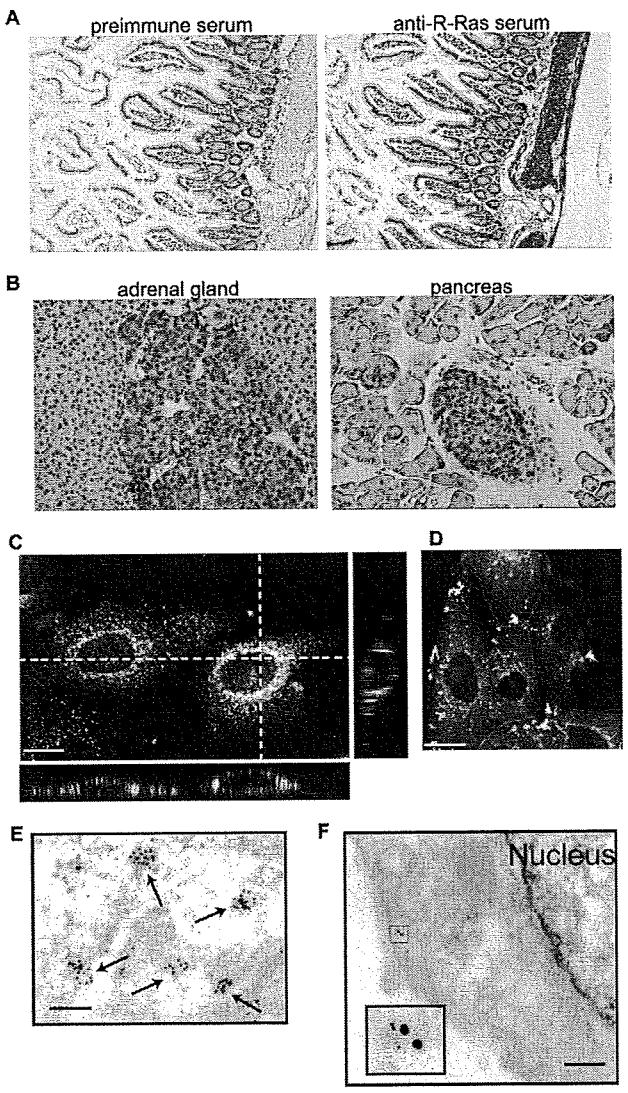

Figure 1. Tissue distribution and subcellular localization of R-Ras. (A) Immunohistochemistry analysis of mouse intestine with preimmune (left) or anti-R-Ras serum (right). Bound antibodies were detected with diaminobenzidine tetrahydrochloride, and the nuclei were counterstained with hematoxylin. Note the staining of the smooth muscle cell layer. (B) Immunohistochemistry of the mouse adrenal gland and pancreas. Note the staining of the adrenal medulla and Langerhans' islands. MDCK cells were fixed in 3.7% formaldehyde and methanol (C) or 4% paraformaldehyde (D) as described in the text, stained with the anti-R-Ras serum and the Alexa 488-coupled anti-rabbit IgG antibody, and observed with a confocal fluorescent microscope. Twenty-five XY images were obtained from the bottom to the top of the cells to prepare the stacked XY image. Cross sections are also shown at the dotted lines. Bar, 10 μm. (E) Immunoelectron micrograph of a MDCK cell stained with anti-R-Ras serum before detection with anti-rabbit IgG labeled with 10-nm gold particles. Bar, 100 nm. (F) Immunoelectron micrograph of a MDCK cell expressing an endosomal marker protein, AcGFP-Endo. Cells were double-stained with anti-R-Ras rabbit serum and anti-GFP mouse mAb JL-8, which were detected with anti-rabbit IgG labeled with 5-nm gold particles and anti-mouse IgG labeled with 10-nm gold particles, respectively. Inset depicts the magnified image of the gold particles. Bar, 100 nm.

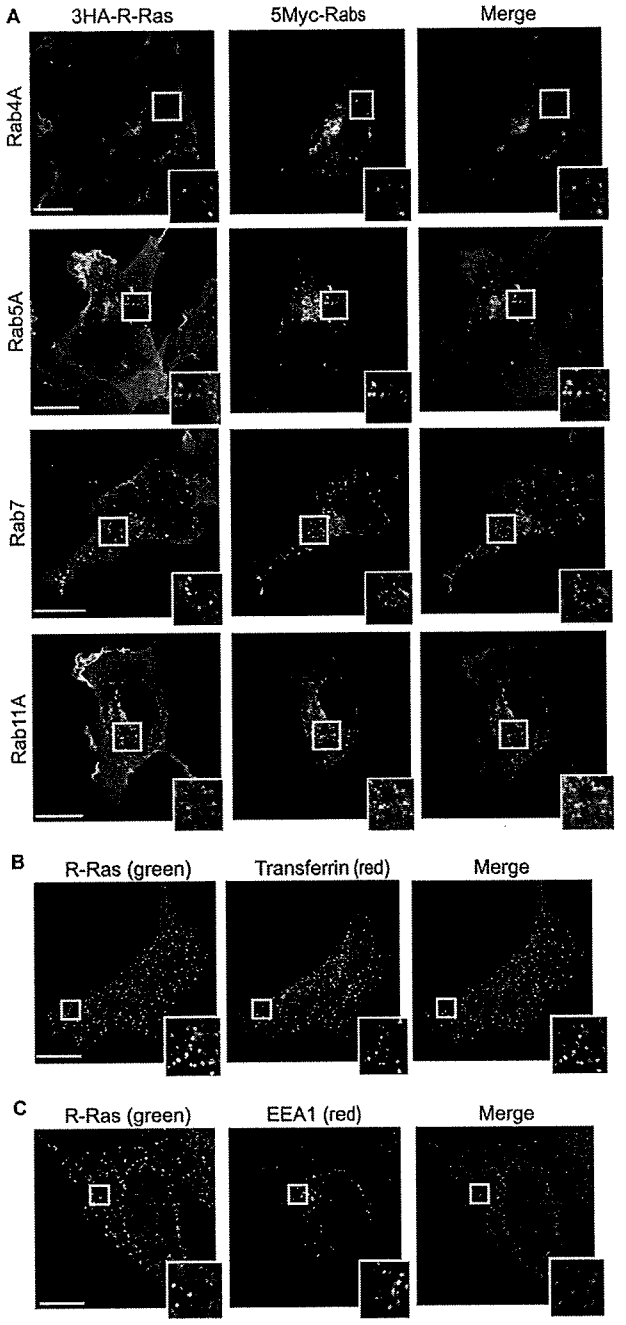

Figure 2. Colocalization of R-Ras with early and recycling endosome markers. (A) Cos7 cells expressing 3HA-tagged R-Ras and 5Myc-tagged Rab4A (early and recycling endosome marker), Rab5A (early endosome marker), Rab7 (late endosome marker), or Rab11A (recycling endosome marker) were double stained with anti-HA and anti-Myc antibodies and then observed with a laser-scanning confocal microscope. In the merged images, the red and green areas indicate anti-Myc and anti-HA antibodies, respectively. Bar, 10 μm. Outlined regions were enlarged and are shown in the insets. (B) Cos7 cells were incubated with Alexa-568-conjugated transferrin for 60 min and then stained with anti-R-Ras serum. (C) Cos7 cells were double stained with anti-R-Ras serum and anti-EEA1 antibody. Bar, 10 μm. Outlined regions were enlarged and are shown in the insets.

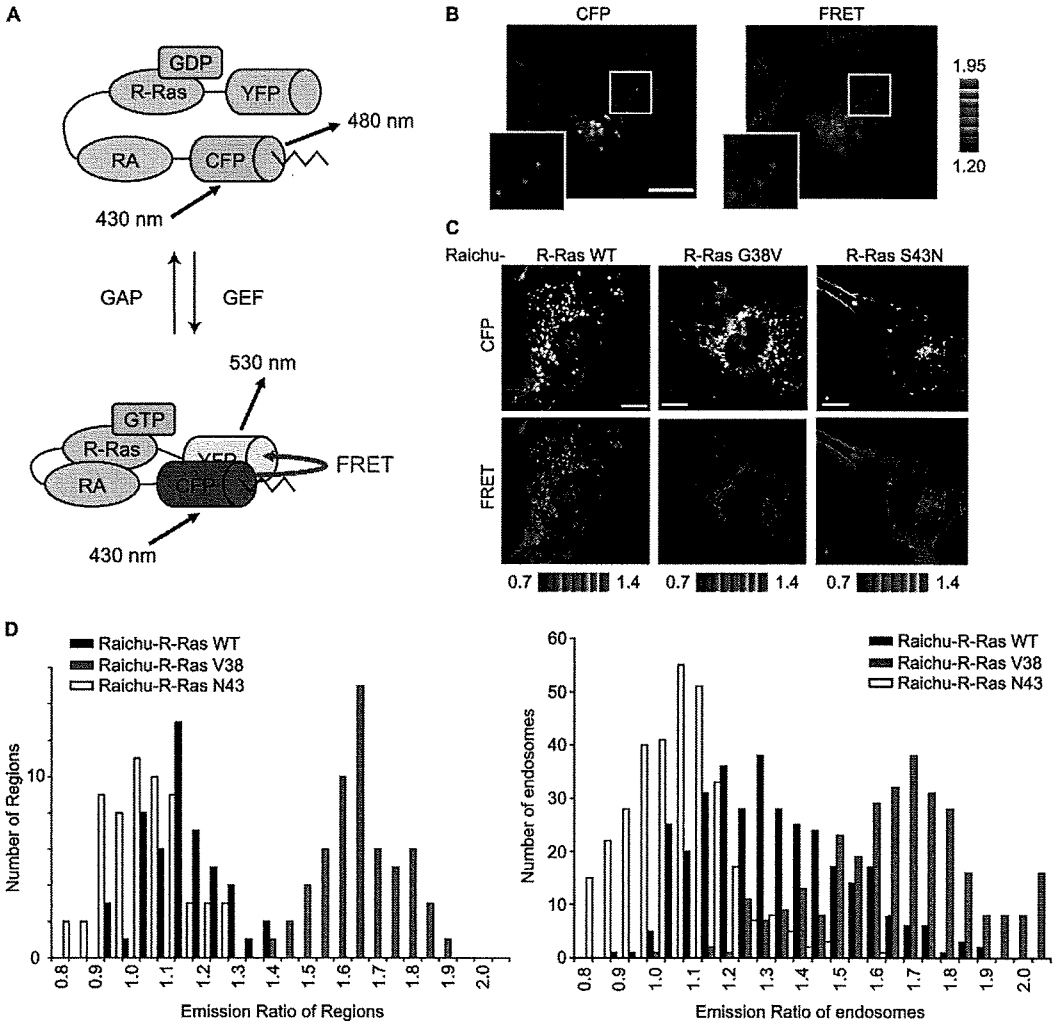

Figure 3. High R-Ras activity on the endosomes. (A) Schematic representation of the Raichu-R-Ras probe. Raichu-R-Ras consisted of a modified YFP designated as Venus, R-Ras, the RA domain (RA) of RalGDS, a modified CFP designated as SECFP, and the carboxy-terminal hypervariable region of R-Ras (indicated by the zigzag lines). On R-Ras activation, the intramolecular binding of R-Ras to the RA domain brings CFP into proximity with YFP, evoking YFP-derived fluorescence by the sensitized FRET. (B) A Cos7 cell expressing Raichu-R-Ras was imaged for CFP (excitation 430 nm/emission 480 nm) and YFP (excitation 430 nm/emission 530 nm). The images of the ratio (YFP versus CFP) were generated to represent the level of FRET. The upper and lower limits of the ratio range are shown on the right. Outlined regions are shown enlarged in the insets. Bar, 10 μm. (C) Cos7 cells expressing Raichu-R-Ras and its mutants were imaged with a confocal microscope. Bar, 10 μm. (D) FRET efficiency (YFP/CFP ratio) of Raichu-R-Ras, Raichu-R-Ras G38V, and Raichu-R-Ras S43N at the plasma membrane (left) and on the endosomes (right). For the endosomes, regions that exhibited higher CFP intensity than an appropriate threshold level were selected, and their YFP and CFP intensities were obtained. For the plasma membrane, three appropriate regions were arbitrarily selected, and the averages of their YFP and CFP intensities were obtained. Data from at least seven cells are shown in the histograms.

Development of a Probe for R-Ras, Raichu-R-Ras

The unexpected observation that R-Ras was enriched on the endosomes urged us to investigate the role played by R-Ras on endosomes. For this purpose, we developed a series of FRET probes for the live-cell imaging of R-Ras activity. For the sake of brevity, only the results obtained with the Raichu-205X probe (hereafter referred to as "Raichu-R-Ras") are described here, because this probe performed best among those tested. From the amino terminus, Raichu-R-Ras includes a modified YFP designated as Venus, human R-Ras (aa 1-199), the Ras-association domain of RalGDS (aa 785-871), a modified CFP referred to as SECFP, and the carboxy-terminal hypervariable region of R-Ras (aa 195-218) (Figure 3A). Raichu-R-Ras fulfills most requirements for a FRET probe as described in the Supplemental Material and Supplemental Figure S3.

Activation of R-Ras on Endosomes

Using Raichu-R-Ras, we visualized R-Ras activity in living Cos7 cells. The distribution of the Raichu-R-Ras probe was indistinguishable from that of the authentic R-Ras: The probe was enriched on the endosomes, but also localized diffusely on the plasma membrane (Figure 3B, Supplemental Figure S4, and Supplemental Movie 2). R-Ras activity, as visualized by the FRET level, was higher on the endosomes than on the plasma membrane. The high R-Ras activity observed on endosomes was more clearly observed with a

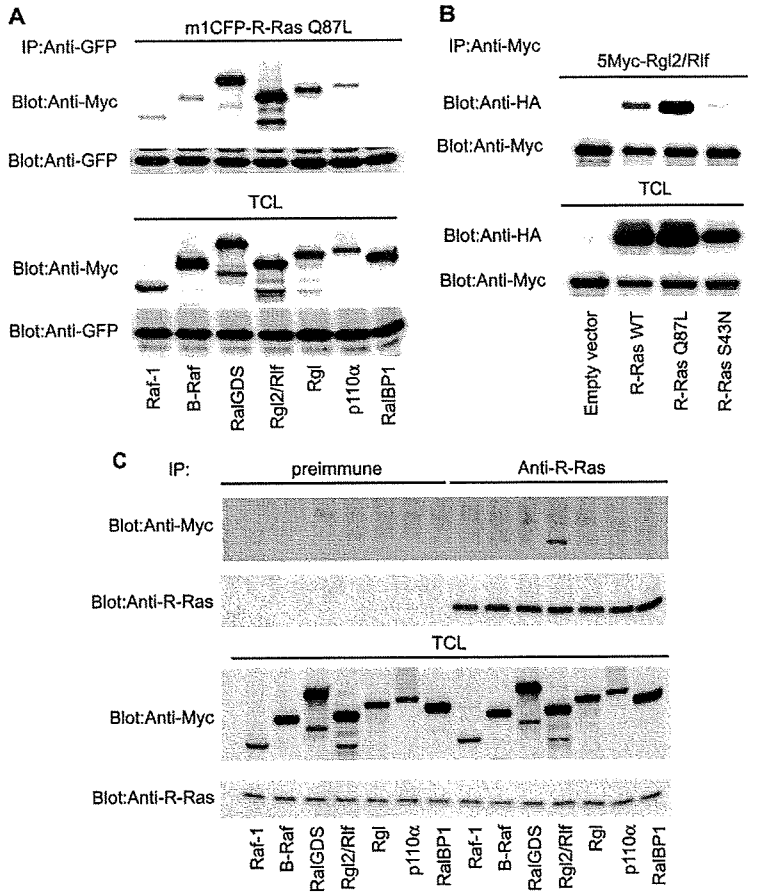

Figure 4. Binding of R-Ras to Rgl2/Rlf. (A) Cos7 cells expressing mCFP-tagged R-Ras-Q87L and the Myc-tagged effector proteins indicated at the bottom of the panel were used for the analysis. In p110α expression, p85α was used for coexpression to stabilize the PI3K heterodimer complex. From the cell lysates, GFP-tagged proteins were immunoprecipitated, and bound proteins were analyzed by immunoblotting with anti-Myc mAb or anti-GFP mAb. (B) Cos7 cells expressing HA-tagged R-Ras mutants and Myc-tagged Rgl2/Rlf were lysed and analyzed as described in A. (C) Endogenous R-Ras protein was immunoprecipitated with anti-R-Ras serum from Cos7 cells expressing the Myc-tagged effector proteins. The immunoprecipitates were analyzed as described in A. Preimmune serum was used as a control.

spinning disk confocal unit (Figure 3C). To exclude the possibility that the high FRET level on the endosomes was caused by accumulation of the probe, we used control probes, i.e., Raichu-R-Ras G38V and Raichu-R-Ras S43N, the properties of which are shown in Supplemental Figure S3. The FRET level was diffusely high on both the plasma membrane and on endosomes in cells expressing Raichu-R-Ras G38V (Figure 3, C and D). In contrast, cells expressing Raichu-R-Ras S43N showed low levels of FRET, both on the plasma membrane and on endosomes (Figure 3, C and D). The intensity of the probe on each endosome did not affect the emission ratio of sensitized FRET over CFP in either the Raichu-R-Ras wild type, G38V mutant, or S43N mutant (data not shown). Therefore, these results negated the possibility that the high FRET signal observed on the endosomes of Raichu-R-Ras–expressing cells was caused by an accumulation of the probe. Interestingly, we could not observe remarkable difference in the localization of the wild-type and mutant Raichu-Ras proteins. This is probably because the effector domain of R-Ras-GTP is masked by the Ras-binding domain of the probe and suggests that the localization of the probe was determined primarily by the carboxy terminus of R-Ras.

Endosomal Localization of Rgl2/Rlf, an R-Ras Effector

Next, we attempted to identify the signaling molecules downstream of R-Ras on the endosomes. To this end, we first compared the affinity of R-Ras for Raf-1, B-Raf, RalGDS, Rgl2/Rlf, Rgl, and the p110α subunit of PI3K, all of which are known to bind to a wide range of Ras-family GTPases (Figure 4A). K-Ras and Rap1A were used as controls for the GTPases (Supplemental Figure S5A). In a coimmunoprecipitation assay, a constitutively active mutant of R-Ras (R-Ras Q87L) was found to interact most strongly with three GEFs for Ral, i.e., RalGDS, Rgl, and Rgl2/Rlf, and less strongly with Raf-1, B-Raf, and p110α. These interactions were shown to depend on GTP loading, because the R-Ras Q87L mutant showed a markedly higher affinity for Rgl2/Rlf than did the wild-type protein and the nucleotide-free mutant, R-Ras S43N (Figure 4B). However, it should be noted that the high-affinity binding detected by coimmunoprecipitation does not necessarily indicate the signaling strength between the two associated proteins. Thus, we examined the effect of the activated R-Ras mutant, R-Ras Q87L, on the activity of downstream effectors. In agreement with the coimmunoprecipitation experiments, RalA, RalB, and Akt1 (downstream of p110 PI3K), but not MEK1 (downstream of the Raf proteins), were activated by R-Ras Q87L (Supplemental Figure S5). Next, we used R-Ras antiserum to examine whether the endogenous R-Ras protein is also associated with Ras effectors. Among the effector proteins tested, Rgl2/Rlf exhibited the strongest affinity for endogenous R-Ras (Figure 4C). Finally, we confirmed that Rgl2/Rlf, but not Raf-1 or p110α, colocalized efficiently with R-Ras on the endosomes (Figure 5, A and B). This endosomal colocalization of Rgl2/Rlf with R-Ras was abrogated by the expression of R-RasGAP (Figure 5C). These results strongly suggested that R-Ras is bound to Rgl2/Rlf on endosomes in a GTP-dependent manner.

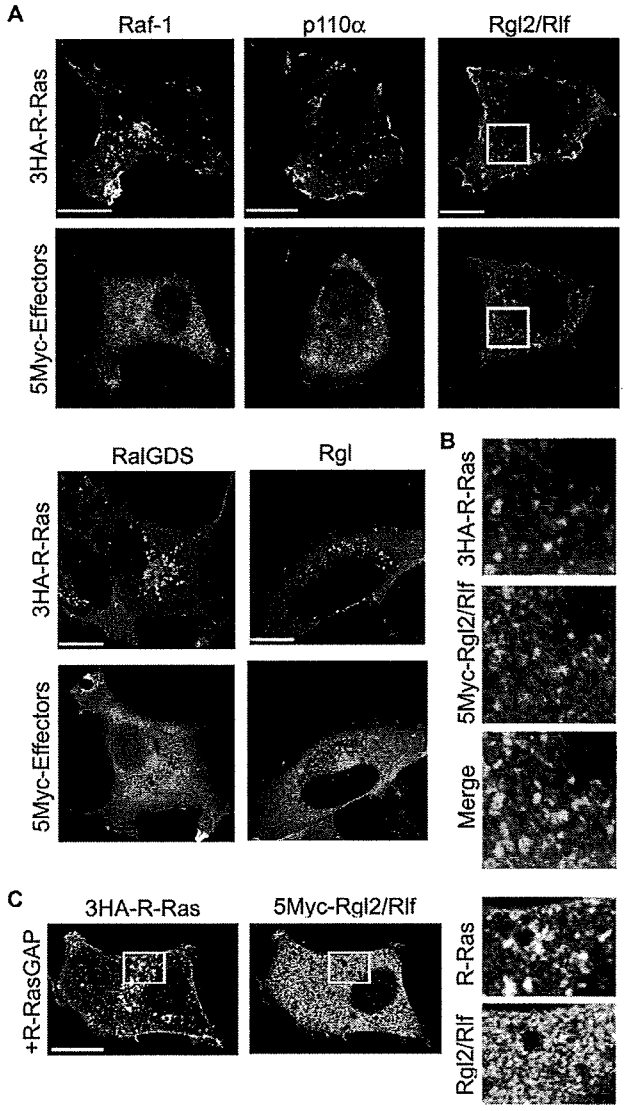

Figure 5. Colocalization of R-Ras with Rgl2/Rlf. (A) Cos7 cells expressing HA-tagged R-Ras and Myc-tagged R-Ras effector proteins were stained with anti-HA and anti-Myc antibodies, and the cells were observed by confocal microscopy. Bar, 10 μm. (B) Enlarged images of the outlined regions in A. In the merged image, green and red indicate 3HA-R-Ras and 5Myc-Rgl2/Rlf, respectively. (C) Cos7 cells expressing HA-tagged R-Ras, Myc-tagged Rgl2/Rlf, and R-RasGAP were stained with anti-HA and anti-Myc antibodies. Right panels are enlarged images of the outlined regions in the left panels.

Regulation of Vesicular RalA Activity by R-Ras

We next addressed the question of whether R-Ras regulates the activities of Ral proteins on the endosomes. In results that were consistent with those of a previous report (Shipitsin and Feig, 2004), RalA and RalB were detected both on the plasma membrane and on endosomes (Supplemental Figure S4C). Because colocalization with R-Ras was clearer in the case of RalA than RalB, we focused on RalA and examined the RalA activity on endosomes by use of Raichu-RalA, a marker for RalA activity (Takaya *et al.*, 2004) (Figure 6). In contrast to the FRET images obtained with Raichu-R-Ras, the FRET level varied significantly among endosomes, suggesting that RalA activity varied among different types of endosomes (Figure 6A). We considered it likely that such differences in RalA activity among endosomes might have depended on the presence of active R-Ras; therefore, we examined RalA activity in cells expressing R-RasGAP or shRNA for R-Ras. Under both conditions, the number of endosomes showing high RalA activity was reduced significantly (Figure 6, B–D). This shRNA-mediated decrease in RalA activity was recovered by the coexpression of exogenous R-Ras, the cDNA of which harbors mutations in the shRNA-binding sequence. The dependence of RalA activity on R-Ras was confirmed by a pull-down assay with the RalA-binding region of RalBP1; the net amount of GTP-RalA was thus shown to have decreased by 20% (Figure 6E). It should be noted that the basal GTP level of RalA is ~7% of total guanine nucleotides bound to RalA (Takaya *et al.*, 2004). Therefore, if we assume based on the immunofluorescence data that the proportion of RalA on the endosomes is significantly smaller than that at the plasma membrane, a 20% decrease in the net amount of GTP-RalA seemed to be consistent with the significant reduction in the number of endosomes showing a high GTP-RalA level, as demonstrated by Raichu-RalA. Finally, we found that knockdown of Rgl2/Rlf profoundly decreased the RalA activity on the endosomes, suggesting that the R-Ras–Rgl2/Rlf complex is the principal activator of RalA on the endosomes (Figure 6F).

Requirement of R-Ras and RalA for Calcium-dependent Exocytosis

It has been reported that RalA is engaged in calcium-triggered exocytosis (Moskalenko *et al.*, 2002; Vitale *et al.*, 2005), which prompted us to examine the role played by R-Ras in the same process. YFP-tagged NPY and rat growth hormone (rGH) were used as markers of exocytosis (Nagai *et al.*, 2002; Matsuno *et al.*, 2005) (Figure 7 and Supplemental Figure S4C). In PC12 cells, depolarization-induced NPY secretion was as significantly inhibited by the expression of active R-Ras (Q87L) and R-RasGAP as by the expression of active RalA (G23V) and Rab11a (Q70L). The expression levels of recombinant proteins were examined by a quantitative immunoblotting analysis (Supplemental Figure S6). Because the expression of Rab11a T22N was less than R-Ras or RalA mutants, the ineffectiveness of this particular mutant might be ascribable to its low expression level. The role played by R-Ras and RalA was further confirmed with small interfering RNA (siRNA) (Figure 7B). The reduction of R-Ras and RalA inhibited depolarization-induced NPY secretion to a similar extent. Among the three Ral GEFs knocked down by siRNA, only the reduction of Rgl2/Rlf had an inhibitory effect on NPY secretion (Figure 7C). In GH3 pituitary adenoma cells, in which the level of expression of endogenous R-Ras was found to be low, the exogenous expression of R-Ras significantly enhanced the depolarization-induced exocytosis of both rGH and NPY (Figure 7D). The enhancement by R-Ras was abrogated by the knockdown of either R-Ras or RalA (Figure 7E). These results demonstrated that R-Ras is involved in depolarization-induced exocytosis, most likely due to the activation of Ral proteins. Furthermore, the finding that not only inhibition but also constitutive activation of R-Ras inhibits exocytosis suggests that the on-off cycle of R-Ras is required for this process.

DISCUSSION

We propose the following scenario for the role of R-Ras on endosomes: 1) R-Ras is activated on the surface of recycling and early endosomes, and it remains active on the vesicles

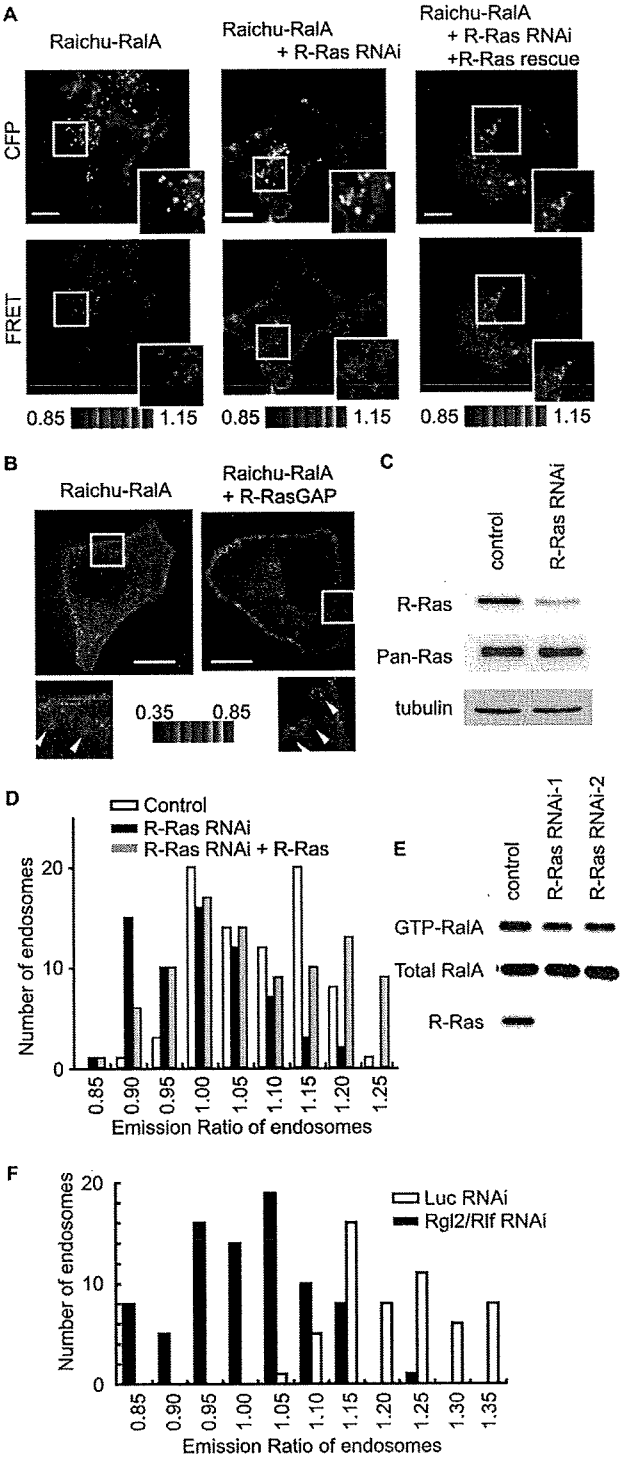

Figure 6. Effect of R-Ras knockdown on RalA activity on the endosomes. (A) Cos7 cells were transfected with expression vectors as indicated at the top of the panel. For knockdown, we used pSuper-R-Ras, an shRNA vector. For the rescue from knockdown, an R-Ras mutant resistant to the shRNA vector was expressed. Sixty hours after transfection, CFP and FRET images were obtained with a spinning confocal microscope. (B) MDCK cells were transfected with expression vectors as indicated at the top of the panel and imaged 20 h after transfection as in A. Outlined regions were enlarged and are shown in the insets. Arrowheads indicate representative vesicles. Bar, 10 μm. (C) Cells transfected with an empty pSuper vector and pSuper-R-Ras were selected as described in A, and the proteins were analyzed by immunoblotting with the antibodies shown on the left. (D) Histogram of the FRET level of Raichu-RalA on the endosomes. The histograms were drawn from the data obtained from 79 endosomes in four Cos7 cells, those obtained from 66 endosomes in six pSuper-R-Ras–expressing Cos7 cells and those obtained from 89 endosomes in nine Cos7 cells expressing both pSuper-R-Ras and pCXN2-5Myc-R-Ras-rRNAi. (E) HeLa cells were transfected with control siRNA or two different siRNAs for R-Ras. After 72 h, GTP-RalA levels in the cells were analyzed by Bos' pull-down method with GST-RalBP1-RBD. The knockdown of R-Ras was also confirmed by immunoblotting. (F) The histograms were drawn from the data obtained from 55 endosomes in two Raichu-RalA-expressing Cos7 cells transfected with siRNA for luciferase and those obtained from 83 endosomes in three Raichu-RalA–expressing Cos7 cells transfected with siRNA for Rgl2/Rlf.

derived from these endosomes. 2) The active R-Ras on these vesicles recruits Ral GEF(s). Among the candidate proteins, Rgl2/Rlf is the most plausible, because R-Ras activates both Rgl and Rgl2/Rlf more efficiently than it does RalGDS (Rodriguez-Viciana *et al.*, 2004), and also because the endogenous R-Ras was found to colocalize with Rgl2/Rlf (Figure 5). However, other Ral GEFs that are also known to bind to R-Ras (Nancy *et al.*, 1999; Shao and Andres, 2000; Rodriguez-Viciana *et al.*, 2004) may be recruited to R-Ras on endosomes in other cell types. 3) These R-Ras-recruited Ral GEFs on the endosomes activate RalA, followed by the recruitment of RalA effectors to the endosomes. Among these effectors is Exo84, a component of the exocyst complex, which marks a microdomain at the plasma membrane as a delivery site for exocytotic vesicles (Grindstaff *et al.*, 1998; Yeaman *et al.*, 2001; Inoue *et al.*, 2003). 4) The R-Ras-loaded vesicles from endosomes are tethered to the plasma membrane via the exocyst complex. It has been demonstrated that the interaction between RalA and the exocyst complex is essential for exocytosis (Moskalenko *et al.*, 2002; Polzin *et al.*, 2002; Shipitsin and Feig, 2004), and the inhibition of the exocyst complex has been shown to impair calcium-triggered exocytosis (Tsuboi *et al.*, 2005). Therefore, our observations that R-Ras was required for the calcium-induced secretion of NPY and rGH (Figure 7) are suggestive of the positive role played by R-Ras in the formation of the exocyst complex.

Another prediction contained in our model, but not directly assessed, is that RalA regulates the assembly of the exocyst complex, both on the vesicles and on the plasma membrane, by means of binding to different components of the exocyst complex: RalA interacts not only with Exo84 but also with Sec5, another component of the exocyst complex (Feig, 2003). Sec5 is primarily present on the plasma membrane, whereas Exo84 is localized primarily on the vesicles (Moskalenko *et al.*, 2003). In this context, it should be noted that RalA is activated on the plasma membrane either by Ras-dependent or by calcium-dependent pathways (Hofer *et al.*, 1998; Wolthuis and Bos, 1999). Hence, the tethering of vesicles may be promoted by the two portions of the exocyst complex, both of which are anchored to the lipid membranes via RalA. One portion consists of subunits containing Exo84 and is anchored to the endosomes and/or the vesicles and endosomes by R-Ras-activated RalA, whereas the other portion consists of subunits containing Sec5, and it is anchored to the plasma membrane by RalA activated by either Ras or calcium. The results have thus far suggested that the high activity of R-Ras and RalA on the surface of vesicles is constitutive rather than stimulation regulated. Therefore, RalA activity at the plasma membrane, but not that on

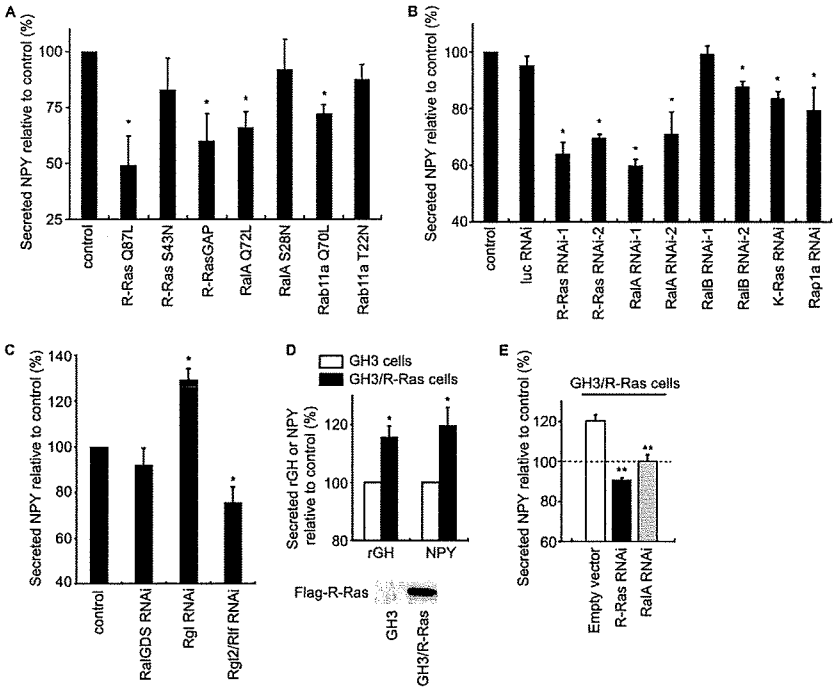

Figure 7. Requirement of both R-Ras and RalA for depolarization-induced exocytosis. (A) PC12 cells were transfected with pVenus-NPY together with the indicated constructs. Sixty hours after transfection, the cells were stimulated with high-potassium saline for 20 min. The efficiency of NPY-Venus secretion was determined as the ratio of NPY-Venus present in the medium versus that remaining in the cell lysates. The values were normalized to a vector control. Error bars indicate the SD from at least three experiments. The symbols indicate the results of *t* test analysis; *p < 0.002 compared with the control. (B and C) PC12 cells were transfected with pVenus-NPY and siRNA for luciferase, R-Ras, RalA, RalB, RalGDS, Rgl, or Rgl2/Rlf. NPY secretion upon depolarization was examined as described in A. Error bars indicate the SD from at least three experiments. The symbols indicate the results of *t* test analysis; *p < 0.001 compared with the control. (D) GH3 cells and GH3/R-Ras cells were transfected with expression vectors for NPY-Venus or EYFP-GH1. Depolarization-induced secretion was monitored as described in A. The symbols indicate the results of *t* test analysis; *p < 0.001 compared with the control. (E) GH3/R-Ras cells were transfected with expression vectors for NPY-Venus and an shRNA vector for R-Ras, or RalA. Depolarization-induced secretion of NPY was examined as described in A. The symbols indicate the results of *t* test analysis; **p < 0.001 compared with the control (GH3/R-Ras cells).

endosomes, may play a regulatory role in the assembly of the complete exocyst complex. In agreement with this view, we have shown that RalA is locally activated in the nascent lamellipodia of epidermal growth factor (EGF)-stimulated or migrating cells (Takaya *et al.*, 2004). Because exocytosis plays critical roles in EGF-induced membrane ruffling and cell migration (Bretscher and Aguado-Velasco, 1998; Schmoranzer *et al.*, 2003; Proux-Gillardeaux *et al.*, 2005; Tayeb *et al.*, 2005), RalA activation at the site of the membrane protrusion may indicate its role in the transport of lipid bilayer and/or integral proteins via exocytosis.

In agreement with the results of a previous report showing that RalA but not RalB regulates the delivery of E-cadherin in MDCK cells (Shipitsin and Feig, 2004), we found that only RalA was involved in calcium-triggered exocytosis (Figure 7). This difference between the two Ral proteins with respect to their involvement in exocytosis may be ascribable not only to the low binding affinity of RalB to Sec5 (Shipitsin and Feig, 2004) but also to the predominant localization of RalB on the plasma membrane (Shipitsin and Feig, 2004; Lim *et al.*, 2005).

Currently, the mechanism underlying the high R-Ras activity on the endosomes remains unknown. A dominant-negative mutant of R-Ras has been shown to be more enriched on endosomes than is the wild-type protein (Furuhjelm and Peranen, 2003). Because a dominant-negative mutant of Ras family GTPases sequesters GEFs (Feig, 1999), these observations strongly suggest that the GEFs for R-Ras are enriched on endosomes. In contrast to RalA on the vesicles, the activity of R-Ras on the vesicles seems constant (Figures 3C and 6A). Thus, R-Ras may be activated as soon as nascent R-Ras is recruited to the vesicles and inactivated when the vesicles are fused to the plasma membrane. Although none of the GEFs for R-Ras (i.e., RasGRF1, CalDAG-GEF-I/RasGRP2, CalDAG-GEF-II/RasGRP1, CalDAG-GEF-III/RasGRP3, and C3G) have been shown to localize on the endosomes (Ohba *et al.*, 2000), this failure to detect GEFs on the endosomes may simply reflect a lack of high-affinity antibodies that could be applied for immunostaining. Interestingly, GAPs for R-Ras seem to localize primarily on the plasma membrane (Anderson *et al.*, 1990; Margolis *et al.*, 1990; Cozier *et al.*, 2003; Oinuma *et al.*, 2004). Thus, R-Ras would be expected to be inactivated when it is transported from the endosomes to the plasma membrane. This inactivation of R-Ras might serve to liberate the components of the exocyst complex and send them back into the cytoplasm or to send R-Ras back to the endosomes from the plasma membrane.

Previous studies have implicated R-Ras in the activation of integrin (Zhang *et al.*, 1996; Keely *et al.*, 1999; Berrier *et al.*, 2000; Self *et al.*, 2001; Oinuma *et al.*, 2006) and also in cell migration and adhesion (Nakada *et al.*, 2005; Wozniak *et al.*, 2005); however, the molecular mechanisms underlying these phenomena remain elusive. Our finding that the R-Ras-Rgl2/Rlf-RalA pathway regulates exocytosis may account for some of these biological activities of R-Ras. It is already known that the inhibition of exocytosis impairs integrin recycling and thereby also cell migration and cell adhesion (Proux-Gillardeaux *et al.*, 2005; Tayeb *et al.*, 2005). Hence, the inhibition of integrin by the suppression of R-Ras might initially be caused by the disruption of exocytosis. Although no direct evidence supporting the involvement of RalA in the recycling of integrin has yet been reported, Ral proteins have been shown to be implicated in cell migration (Gildea *et al.*, 2002; Takaya *et al.*, 2004; Oxford *et al.*, 2005), a process in which integrin is thought to be coordinately activated and inactivated. Therefore, it is reasonable to speculate that the R-Ras-Rgl2/Rlf-RalA pathway is involved in the recycling of integrin and thereby also in the regulation of integrin activity.

In conclusion, we observed high R-Ras activity on early and recycling endosomes. This high R-Ras activity recruits Rlf/Rgl2 and thereby activates RalA, followed by the assembly of a portion of the exocyst complex. Importantly, in

addition to RalA, other low-molecular-weight GTPases belonging to different families (i.e., TC10, Arf6, and Rab11) are also known to interact with the exocyst complex (Prigent *et al.*, 2003; Inoue *et al.*, 2003; Zhang *et al.*, 2004; Wu *et al.*, 2005). Further study will be needed to determine whether these GTPases of different families coordinately regulate the exocyst complex on the same endosomes, or whether there are distinct classes of endosomes containing only some of these GTPases. It would be of particular importance to examine the dynamic activity changes of these GTPases during the vesicular transport, which would be best examined by FRET-based imaging techniques used here.

ACKNOWLEDGMENTS

We thank L. A. Feig, R. Y. Tsien, Y. Fukui, K. Kaibuchi, A. Kikuchi, S. Kuroda, B. J. Mayer, N. Minato, A. Miyawaki, and Y. Takai for the provision of reagents and N. Yoshida, N. Fujimoto, and K. Fukuhara for technical assistance. This work was supported by grants-in-aid for scientific research and for cancer research from the Ministry of Education, Science, Sports and Culture of Japan, and by a grant from the Health Science Foundation of Japan. A.T. was supported by Research Fellowships from the Japan Society for the Promotion of Science for Young Scientists.

REFERENCES

Akagi, T., Sasai, K., and Hanafusa, H. (2003). Refractory nature of normal human diploid fibroblasts with respect to oncogene-mediated transformation. Proc. Natl. Acad. Sci. USA *100*, 13567–13572.

Anderson, D., Koch, C. A., Grey, L., Ellis, C., Moran, M. F., and Pawson, T. (1990). Binding of SH2 domains of phospholipase C gamma 1, GAP, and Src to activated growth factor receptors. Science *250*, 979–982.

Aoki, K., Nakamura, T., Fujikawa, K., and Matsuda, M. (2005). Local phosphatidylinositol 3,4,5-trisphosphate accumulation recruits Vav2 and Vav3 to activate Rac1/Cdc42 and initiate neurite outgrowth in nerve growth factor-stimulated PC12 cells. Mol. Biol. Cell *16*, 2207–2217.

Berrier, A. L., Mastrangelo, A. M., Downward, J., Ginsberg, M., and LaFlamme, S. E. (2000). Activated R-ras, Rac1, PI 3-kinase and PKCepsilon can each restore cell spreading inhibited by isolated integrin beta1 cytoplasmic domains. J. Cell Biol. *151*, 1549–1560.

Bretscher, M. S., and Aguado-Velasco, C. (1998). EGF induces recycling membrane to form ruffles. Curr. Biol. *8*, 721–724.

Cox, A. D., Brtva, T. R., Lowe, D. G., and Der, C. J. (1994). R-Ras induces malignant, but not morphologic, transformation of NIH3T3 cells. Oncogene *9*, 3281–3288.

Cozier, G. E., Bouyoucef, D., and Cullen, P. J. (2003). Engineering the phosphoinositide-binding profile of a class I pleckstrin homology domain. J. Biol. Chem. *278*, 39489–39496.

Feig, L. A. (1999). Tools of the trade: use of dominant-inhibitory mutants of Ras-family GTPases. Nat. Cell Biol. *1*, E25–E27.

Feig, L. A. (2003). Ral-GTPases: approaching their 15 minutes of fame. Trends Cell Biol. *13*, 419–425.

Finger, F. P., Hughes, T. E., and Novick, P. (1998). Sec3p is a spatial landmark for polarized secretion in budding yeast. Cell *92*, 559–571.

Friedrich, G. A., Hildebrand, J. D., and Soriano, P. (1997). The secretory protein Sec8 is required for paraxial mesoderm formation in the mouse. Dev. Biol. *192*, 364–374.

Furuhjelm, J., and Peranen, J. (2003). The C-terminal end of R-Ras contains a focal adhesion targeting signal. J. Cell Sci. *116*, 3729–3738.

Gildea, J. J., Harding, M. A., Seraj, M. J., Gulding, K. M., and Theodorescu, D. (2002). The role of Ral A in epidermal growth factor receptor-regulated cell motility. Cancer Res. *62*, 982–985.

Gonzalez-Garcia, A., Pritchard, C. A., Paterson, H. F., Mavria, G., Stamp, G., and Marshall, C. J. (2005). RalGDS is required for tumor formation in a model of skin carcinogenesis. Cancer Cell *7*, 219–226.

Gotoh, T., Niino, Y., Tokuda, M., Hatase, O., Nakamura, S., Matsuda, M., and Hattori, S. (1997). Activation of R-Ras by Ras-guanine nucleotide-releasing factor. J. Biol. Chem. *272*, 18602–18607.

Grindstaff, K. K., Yeaman, C., Anandasabapathy, N., Hsu, S. C., Rodriguez-Boulan, E., Scheller, R. H., and Nelson, W. J. (1998). Sec6/8 complex is recruited to cell-cell contacts and specifies transport vesicle delivery to the basal-lateral membrane in epithelial cells. Cell *93*, 731–740.

Gromley, A., Yeaman, C., Rosa, J., Redick, S., Chen, C. T., Mirabelle, S., Guha, M., Sillibourne, J., and Doxsey, S. J. (2005). Centriolin anchoring of exocyst and SNARE complexes at the midbody is required for secretory-vesicle-mediated abscission. Cell *123*, 75–87.

Hamad, N. M., Elconin, J. H., Karnoub, A. E., Bai, W., Rich, J. N., Abraham, R. T., Der, C. J., and Counter, C. M. (2002). Distinct requirements for Ras oncogenesis in human versus mouse cells. Genes Dev. *16*, 2045–2057.

Hofer, F., Berdeaux, R., and Martin, G. S. (1998). Ras-independent activation of Ral by a Ca(2+)-dependent pathway. Curr. Biol. *8*, 839–842.

Huff, S. Y., Quilliam, L. A., Cox, A. D., and Der, C. J. (1997). R-Ras is regulated by activators and effectors distinct from those that control Ras function. Oncogene *14*, 133–143.

Inoue, M., Chang, L., Hwang, J., Chiang, S. H., and Saltiel, A. R. (2003). The exocyst complex is required for targeting of Glut4 to the plasma membrane by insulin. Nature *422*, 629–633.

Keely, P. J., Rusyn, E. V., Cox, A. D., and Parise, L. V. (1999). R-Ras signals through specific integrin alpha cytoplasmic domains to promote migration and invasion of breast epithelial cells. J. Cell Biol. *145*, 1077–1088.

Komatsu, M., and Ruoslahti, E. (2005). R-Ras is a global regulator of vascular regeneration that suppresses intimal hyperplasia and tumor angiogenesis. Nat. Med. *11*, 1346–1350.

Kurokawa, K., Itoh, R. E., Yoshizaki, H., Nakamura, T., and Matsuda, M. (2004a). Coactivation of Rac1 and Cdc42 at lamellipodia and membrane ruffles induced by epidermal growth factor. Mol. Biol. Cell *15*, 1003–1010.

Kurokawa, K., Takaya, A., Terai, K., Fujioka, A., and Matsuda, M. (2004b). Visualizing the signal transduction pathways in living cells with GFP-based FRET probes. Acta Histochem. Cytochem. *37*, 347–355.

Lim, K. H., Baines, A. T., Fiordalisi, J. J., Shipitsin, M., Feig, L. A., Cox, A. D., Der, C. J., and Counter, C. M. (2005). Activation of RalA is critical for Ras-induced tumorigenesis of human cells. Cancer Cell *7*, 533–545.

Lipschutz, J. H., and Mostov, K. E. (2002). Exocytosis: the many masters of the exocyst. Curr. Biol. *12*, R212–R214.

Lowe, D. G., Capon, D. J., Delwart, E., Sakaguchi, A. Y., Naylor, S. L., and Goeddel, D. V. (1987). Structure of the human and murine R-ras genes, novel genes closely related to ras proto-oncogenes. Cell *48*, 137–146.

Margolis, B., Li, N., Koch, A., Mohammadi, M., Hurwitz, D. R., Zilberstein, A., Ullrich, A., Pawson, T., and Schlessinger, J. (1990). The tyrosine phosphorylated carboxy terminus of the EGF receptor is a binding site for GAP and PLC-gamma. EMBO J. *9*, 4375–4380.

Marte, B. M., Rodriguez-Viciana, P., Wennstrom, S., Warne, P. H., and Downward, J. (1997). R-Ras can activate the phosphoinositide 3-kinase but not the MAP kinase arm of the Ras effector pathways. Curr. Biol. *7*, 63–70.

Matsuno, A., Mizutani, A., Itoh, J., Takekoshi, S., Nagashima, T., Okinaga, H., Takano, K., and Osamura, R. Y. (2005). Establishment of stable GH3 cell line expressing enhanced yellow fluorescein protein-growth hormone fusion protein. J. Histochem. Cytochem. *53*, 1177–1180.

Mochizuki, N., Yamashita, S., Kurokawa, K., Ohba, Y., Nagai, T., Miyawaki, A., and Matsuda, M. (2001). Spatio-temporal images of growth-factor-induced activation of Ras and Rap1. Nature *411*, 1065–1068.

Moskalenko, S., Henry, D. O., Rosse, C., Mirey, G., Camonis, J. H., and White, M. A. (2002). The exocyst is a Ral effector complex. Nat. Cell Biol. *4*, 66–72.

Moskalenko, S., Tong, C., Rosse, C., Mirey, G., Formstecher, E., Daviet, L., Camonis, J., and White, M. A. (2003). Ral GTPases regulate exocyst assembly through dual subunit interactions. J. Biol. Chem. *278*, 51743–51748.

Murthy, M., Garza, D., Scheller, R. H., and Schwarz, T. L. (2003). Mutations in the exocyst component Sec5 disrupt neuronal membrane traffic, but neurotransmitter release persists. Neuron *37*, 433–447.

Nagai, T., Ibata, K., Park, E. S., Kubota, M., Mikoshiba, K., and Miyawaki, A. (2002). A variant of yellow fluorescent protein with fast and efficient maturation for cell-biological applications. Nat. Biotechnol. *20*, 87–90.

Nakada, M., Niska, J. A., Tran, N. L., McDonough, W. S., and Berens, M. E. (2005). EphB2/R-Ras signaling regulates glioma cell adhesion, growth, and invasion. Am. J. Pathol. *167*, 565–576.

Nakashima, S., Morinaka, K., Koyama, S., Ikeda, M., Kishida, M., Okawa, K., Iwamatsu, A., Kishida, S., and Kikuchi, A. (1999). Small G protein Ral and its downstream molecules regulate endocytosis of EGF and insulin receptors. EMBO J. *18*, 3629–3642.

Nancy, V., Wolthuis, R. M., de Tand, M. F., Janoueix-Lerosey, I., Bos, J. L., and de Gunzburg, J. (1999). Identification and characterization of potential effector molecules of the Ras-related GTPase Rap2. J. Biol. Chem. *274*, 8737–8745.

Nishigaki, M., Aoyagi, K., Danjoh, I., Fukaya, M., Yanagihara, K., Sakamoto, H., Yoshida, T., and Sasaki, H. (2005). Discovery of aberrant expression of R-RAS by cancer-linked DNA hypomethylation in gastric cancer using microarrays. Cancer Res. *65*, 2115–2124.

Ohba, Y., Mochizuki, N., Yamashita, S., Chan, A. M., Schrader, J. W., Hattori, S., Nagashima, K., and Matsuda, M. (2000). Regulatory proteins of R-Ras, TC21/R-Ras2, and M-Ras/R-Ras3. J. Biol. Chem. *275*, 20020–20026.

Oinuma, I., Ishikawa, Y., Katoh, H., and Negishi, M. (2004). The Semaphorin 4D receptor Plexin-B1 is a GTPase activating protein for R-Ras. Science *305*, 862–865.

Oinuma, I., Katoh, H., and Negishi, M. (2006). Semaphorin 4D/Plexin-B1-mediated R-Ras GAP activity inhibits cell migration by regulating beta(1) integrin activity(2). J. Cell Biol. *173*, 601–613.

Oxford, G., Owens, C. R., Titus, B. J., Foreman, T. L., Herlevsen, M. C., Smith, S. C., and Theodorescu, D. (2005). RalA and RalB: antagonistic relatives in cancer cell migration. Cancer Res. *65*, 7111–7120.

Polzin, A., Shipitsin, M., Goi, T., Feig, L. A., and Turner, T. J. (2002). Ral-GTPase influences the regulation of the readily releasable pool of synaptic vesicles. Mol. Cell. Biol. *22*, 1714–1722.

Prigent, M., Dubois, T., Raposo, G., Derrien, V., Tenza, D., Rosse, C., Camonis, J., and Chavrier, P. (2003). ARF6 controls post-endocytic recycling through its downstream exocyst complex effector. J. Cell Biol. *163*, 1111–1121.

Proux-Gillardeaux, V., Gavard, J., Irinopoulou, T., Mege, R. M., and Galli, T. (2005). Tetanus neurotoxin-mediated cleavage of cellubrevin impairs epithelial cell migration and integrin-dependent cell adhesion. Proc. Natl. Acad. Sci. USA *102*, 6362–6367.

Quilliam, L.A., Rebhun, J. F., and Castro, A. F. (2002). A growing family of guanine nucleotide exchange factors is responsible for activation of Ras-family GTPases. Prog. Nucleic Acid Res. Mol. Biol. *71*, 391–444.

Rangarajan, A., Hong, S. J., Gifford, A., and Weinberg, R. A. (2004). Species- and cell type-specific requirements for cellular transformation. Cancer Cell *6*, 171–183.

Rey, I., Taylor-Harris, P., van Erp, H., and Hall, A. (1994). R-ras interacts with rasGAP, neurofibromin and c-raf but does not regulate cell growth or differentiation. Oncogene *9*, 685–692.

Rodriguez-Viciana, P., Sabatier, C., and McCormick, F. (2004). Signaling specificity by Ras family GTPases is determined by the full spectrum of effectors they regulate. Mol. Cell. Biol. *24*, 4943–4954.

Schmoranzer, J., Kreitzer, G., and Simon, S. M. (2003). Migrating fibroblasts perform polarized, microtubule-dependent exocytosis towards the leading edge. J. Cell Sci. *116*, 4513–4519.

Self, A. J., Caron, E., Paterson, H. F., and Hall, A. (2001). Analysis of R-Ras signalling pathways. J. Cell Sci. *114*, 1357–1366.

Shao, H., and Andres, D. A. (2000). A novel RalGEF-like protein, RGL3, as a candidate effector for rit and Ras. J. Biol. Chem. *275*, 26914–26924.

Shipitsin, M., and Feig, L. A. (2004). RalA but not RalB enhances polarized delivery of membrane proteins to the basolateral surface of epithelial cells. Mol. Cell. Biol. *24*, 5746–5756.

Spaargaren, M., and Bischoff, J. R. (1994). Identification of the guanine nucleotide dissociation stimulator for Ral as a putative effector molecule of R-ras, H-ras, K-ras, and Rap. Proc. Natl. Acad. Sci. USA *91*, 12609–12613.

Spaargaren, M., Martin, G. A., McCormick, F., Fernandez-Sarabia, M. J., and Bischoff, J. R. (1994). The Ras-related protein R-ras interacts directly with Raf-1 in a GTP-dependent manner. Biochem. J. *300*, 303–307.

Takaya, A., Ohba, Y., Kurokawa, K., and Matsuda, M. (2004). RalA activation at nascent lamellipodia of epidermal growth factor-stimulated Cos7 cells and migrating Madin-Darby canine kidney cells. Mol. Biol. Cell *15*, 2549–2557.

Tayeb, M. A., Skalski, M., Cha, M. C., Kean, M. J., Scaife, M., and Coppolino, M. G. (2005). Inhibition of SNARE-mediated membrane traffic impairs cell migration. Exp. Cell Res. *305*, 63–73.

Tsuboi, T., Ravier, M. A., Xie, H., Ewart, M. A., Gould, G. W., Baldwin, S. A., and Rutter, G. A. (2005). Mammalian exocyst complex is required for the docking step of insulin vesicle exocytosis. J. Biol. Chem. *280*, 25565–25570.

Vega, I. E., and Hsu, S. C. (2001). The exocyst complex associates with microtubules to mediate vesicle targeting and neurite outgrowth. J. Neurosci. *21*, 3839–3848.

Vitale, N., Mawet, J., Camonis, J., Regazzi, R., Bader, M. F., and Chasserot-Golaz, S. (2005). The Small GTPase RalA controls exocytosis of large dense core secretory granules by interacting with ARF6-dependent phospholipase D1. J. Biol. Chem. *280*, 29921–29928.

Wolthuis, R. M., and Bos, J. L. (1999). Ras caught in another affair: the exchange factors for Ral. Curr. Opin. Genet. Dev. *9*, 112–117.

Wozniak, M. A., Kwong, L., Chodniewicz, D., Klemke, R. L., and Keely, P. J. (2005). R-Ras controls membrane protrusion and cell migration through the spatial regulation of Rac and Rho. Mol. Biol. Cell *16*, 84–96.

Wu, S., Mehta, S. Q., Pichaud, F., Bellen, H. J., and Quiocho, F. A. (2005). Sec15 interacts with Rab11 via a novel domain and affects Rab11 localization in vivo. Nat. Struct. Mol. Biol. *12*, 879–885.

Yamamoto, T., Matsui, T., Nakafuku, M., Iwamatsu, A., and Kaibuchi, K. (1995). A novel GTPase-activating protein for R-Ras. J. Biol. Chem. *270*, 30557–30561.

Yeaman, C., Grindstaff, K. K., Wright, J. R., and Nelson, W. J. (2001). Sec6/8 complexes on trans-Golgi network and plasma membrane regulate late stages of exocytosis in mammalian cells. J. Cell Biol. *155*, 593–604.

Zacharias, D. A., Violin, J. D., Newton, A. C., and Tsien, R. Y. (2002). Partitioning of lipid-modified monomeric GFPs into membrane microdomains of live cells. Science *296*, 913–916.

Zhang, X. M., Ellis, S., Sriratana, A., Mitchell, C. A., and Rowe, T. (2004). Sec15 is an effector for the Rab11 GTPase in mammalian cells. J. Biol. Chem. *279*, 43027–43034.

Zhang, Z., Vuori, K., Wang, H., Reed, J. C., and Ruoslahti, E. (1996). Integrin activation by R-ras. Cell *85*, 61–69.

Research article

A cardiac myosin light chain kinase regulates sarcomere assembly in the vertebrate heart

Osamu Seguchi,[1] Seiji Takashima,[2,3] Satoru Yamazaki,[1] Masanori Asakura,[1] Yoshihiro Asano,[2] Yasunori Shintani,[2] Masakatsu Wakeno,[1] Tetsuo Minamino,[2] Hiroya Kondo,[2] Hidehiko Furukawa,[4] Kenji Nakamaru,[4] Asuka Naito,[4] Tomoko Takahashi,[4] Toshiaki Ohtsuka,[4] Koichi Kawakami,[5] Tadashi Isomura,[6] Soichiro Kitamura,[1] Hitonobu Tomoike,[1] Naoki Mochizuki,[1] and Masafumi Kitakaze[1]

[1]Department of Cardiovascular Medicine, National Cardiovascular Center, Suita, Osaka, Japan. [2]Department of Cardiovascular Medicine and [3]Health Care Center, Osaka University Graduate School of Medicine, Suita, Osaka, Japan. [4]Core Technology Research Laboratories, Sankyo Co. Ltd., Shinagawa, Tokyo, Japan. [5]Division of Molecular and Developmental Biology, National Institute of Genetics, Mishima, Shizuoka, Japan. [6]Hayama Heart Center, Hayama, Kanagawa, Japan.

Marked sarcomere disorganization is a well-documented characteristic of cardiomyocytes in the failing human myocardium. Myosin regulatory light chain 2, ventricular/cardiac muscle isoform (MLC2v), which is involved in the development of human cardiomyopathy, is an important structural protein that affects physiologic cardiac sarcomere formation and heart development. Integrated cDNA expression analysis of failing human myocardia uncovered a novel protein kinase, cardiac-specific myosin light chain kinase (cardiac-MLCK), which acts on MLC2v. Expression levels of cardiac-MLCK were well correlated with the pulmonary arterial pressure of patients with heart failure. In cultured cardiomyocytes, knockdown of cardiac-MLCK by specific siRNAs decreased MLC2v phosphorylation and impaired epinephrine-induced activation of sarcomere reassembly. To further clarify the physiologic roles of cardiac-MLCK in vivo, we cloned the zebrafish ortholog z–cardiac-MLCK. Knockdown of z–cardiac-MLCK expression using morpholino antisense oligonucleotides resulted in dilated cardiac ventricles and immature sarcomere structures. These results suggest a significant role for cardiac-MLCK in cardiogenesis.

Introduction

Despite recent advances in pharmacologic and surgical therapies, chronic heart failure (CHF) is still a leading cause of death worldwide (1). Currently, heart transplant is thought to be the most effective therapy for end-stage CHF. However, this approach obviously cannot be used for all of the numerous affected patients and is not suitable for patients with a mild disease state. Therefore, there is increasing demand for new therapeutic targets for CHF.

Cardiomyocytes, the most basic cellular unit of the myocardium, express several sarcomeric proteins, including myosin and actin; abnormalities in these sarcomeric proteins are major causes of idiopathic cardiomyopathies and lead to CHF (2–4). Type II myosin is the major constituent of sarcomeres. In the neck region of this protein, there are binding sites for a pair of myosin light chains, which are called the essential light chain and the regulatory light chain. Among the several paralogs of the myosin regulatory light chain in vertebrates (5), myosin regulatory light chain 2, ventricular/cardiac muscle isoform (MLC2v) is expressed in the myocardium, where it performs specific roles in cardiogenesis by contributing to the formation of sarcomeres and in increasing the Ca^{2+} sensitivity of muscle tension at submaximal Ca^{2+} concentrations (6, 7). Currently, 2 members of the myosin light chain kinase (MLCK) protein family that act on myosin regulatory light chain in muscle cells have been identified, skeletal muscle MLCK (skMLCK) and smooth muscle MLCK (smMLCK) (8). Among these MLCK family members, smMLCK, including nonmuscle isoforms, is distributed ubiquitously in various tissues and contributes to the contraction of smooth muscle and several cell activities. Conversely, skMLCK is thought to localize and function in both cardiac muscle and skeletal muscle (9); to our knowledge, no cardiac-specific MLCK has been reported to date. skMLCK-deficient mice, however, did not show any heart weight, body weight, or heart weight/body weight ratio phenotypes, despite effective knockdown of skMLCK expression (10). Additionally, there were no significant differences between the knockout and wild-type animals in regard to MLC2v phosphorylation, suggesting the existence of as-yet unknown kinases in cardiac muscle cells.

Genome-wide analyses, which have recently become available in a wide range of clinical settings, such as cancer research, allow for a global view of gene expression in certain disease states and the identification of unknown molecules and molecular pathways that can be exploited as novel therapeutic targets. CHF is a candidate disease for this type of genome-wide analysis, because of its heterogeneous properties and previous difficulties identifying responsible genes using other conventional modalities.

In this study, we performed microarray analysis of the failing human myocardium and examined the correlation between the obtained genomic data and the clinical, physiological, and biochemical characteristics of CHF. In this manner, we sought to identify candidate genes that are involved in the pathophysiology of CHF. Consequently, we identified what we believe to be a novel

Nonstandard abbreviations used: ANP, atrial natriuretic peptide; BNP, brain natriuretic peptide; CHF, chronic heart failure; cardiac-MLCK, cardiac-specific MLCK; Dd, end-diastolic dimension; Ds, end-systolic dimension; FS, fractional shortening; hpf, hours postfertilization; MI, myocardial infarction; MLC2v, myosin regulatory light chain 2, ventricular/cardiac muscle isoform; MLCK, myosin light chain kinase; M-mode, motion mode; MO, morpholino antisense oligonucleotide; p-s15MLC, antibodies for phosphorylated MLC2v; PAP, pulmonary arterial pressure; RcMK, antibodies specific for rodent cardiac-MLCK; si-cMK, siRNA targeting cardiac-MLCK; si-smMK, siRNA targeting rat smMLCK; skMLCK, skeletal muscle MLCK; smMLCK, smooth muscle MLCK; tMLC, antibodies for total MLC2v; z-, zebrafish; z-cMKaugMO, MO targeting the AUG translational start site of z-cardiac-MLCK.

Conflict of interest: The authors have declared that no conflict of interest exists.

Citation for this article: *J. Clin. Invest.* **117**:2812–2824 (2007). doi:10.1172/JCI30804.

Table 1
Clinical characteristics of the patients used for microarray analysis

Pt	Age (yr)	Sex	Diagnosis	Operation	Dd (mm)	EF (%)	PAP (mmHg)	ANP (pg/ml)	BNP (pg/ml)
1	53	M	DCM, MI	Batista	88	25	20	25	90.4
2	45	M	DCM	Batista	81	39	45	85	217
3	72	M	DCM	Batista	71	14	25	86	201
4	58	M	MI	Dor	76	–	–	–	–
5	57	M	HCM, MI	Dor	52	44	41	20	80.3
6	69	M	DCM	Batista	86	19	59	100	465
7	40	M	AR	Unknown	76	42	16	52	271
8	75	M	MI	Dor	51	55	–	39	174
9	32	M	DCM	Batista	81	26	26	300	869
10	51	F	Sarcoidosis	Dor	68	35	–	89	339
11	54	M	MI	Dor	63	37	–	84	302
12	58	M	Myocarditis	Dor	77	22	–	800	2,710
N-1	27	M	Normal	–	–	–	–	–	–
N-2	24	M	Normal	–	–	–	–	–	–

AR, aortic regurgitation; DCM, dilated cardiomyopathy; EF, ejection fraction; F, female; HCM, hypertrophic cardiomyopathy; M, male; Pt, patient.

cardiac-specific MLCK (cardiac-MLCK; encoded by *MYLK3*). Phosphorylation of MLC2v by cardiac-MLCK regulated the reassembly of sarcomere structures in cultured neonatal rat cardiomyocytes. Suppression of cardiac-MLCK expression in zebrafish embryos using specific morpholino antisense oligonucleotides (MOs) led to dilation of the cardiac ventricle with incomplete sarcomere formation, suggesting critical roles for cardiac-MLCK in the heart.

Results

Identification of cardiac-MLCK from failing human myocardia using microarray analysis. To identify candidate genes involved in the pathophysiology of CHF, we used an HG-U95 Affymetrix GeneChip to analyze the gene expression profiles of failing myocardial tissues obtained from 12 patients who had undergone cardiac exclusion surgery, such as the Dor or Batista procedures, for end-stage CHF (Table 1). Figure 1A is an overview flowchart for the selection of candidate genes. Compared with those of 2 normal control samples, the expression of 626 probe sets was significantly upregulated in the failing myocardia. Of these, we selected probe sets whose expression levels were positively correlated ($r > 0.7$) with pulmonary arterial pressure (PAP) measurements (129 probe sets) and brain natriuretic peptide (BNP) mRNA levels (194 probe sets). The tissue localization of each selected probe set was then analyzed using the commercially available BioExpress database (Gene Logic Inc.). We selected 10 probe sets, for which the cardiac expression level was at least 10-fold the mean expression level of 24 other tissues, for further analysis. These probe sets represented a set of genes that included atrial natriuretic peptide (ANP), BNP, small muscle protein, and α-actin, all of which are known to be involved in heart failure, cardiac muscle remodeling, and striated muscle function. We calculated the ratios of expression in cardiac muscle to that in skeletal muscle in these probe sets. ANP (36663_at and 73106_s_at), BNP (39215_at), Importin9 (84730_at), and 75678_at exhibited expression levels that were at least 10-fold greater in the heart than in skeletal muscle. Expression levels of 75678_at, for which annotation was not available, were similar to those of ANP and BNP. We hypothesized that this unknown transcript was involved in the pathophysiology of heart failure.

Using 5′-RACE, we identified specific sequences identical to those of NM_182493 (*MYLK3*) located 4 kb upstream of the probe set sequence. The relative expression level of this candidate gene was significantly correlated with the relative PAP value (Figure 1B); in addition, the expression of this gene was restricted to the heart (Figure 1C). A homology search using the transcript sequence, particularly the sequence coding for the C-terminal kinase domain, identified *MYLK3* as a member of the MLCK family. Thus, we named the protein encoded by *MYLK3* "cardiac-MLCK." Two distinct MLCK family genes have been previously reported: *MYLK*, which encodes smMLCK, and *MYLK2*, which encodes skMLCK (8). Domain structure analysis revealed a well-conserved serine/threonine kinase domain that includes an ATP-binding site and an active serine/threonine kinase domain positioned near the C terminus of the cardiac-MLCK protein (Figure 1D). The expression patterns of the MLCK family members were confirmed by Northern blot analysis. As previously described (11), 2 major transcripts of *MYLK* were almost ubiquitously expressed. The larger transcript codes for a nonmuscle isoform of smMLCK generated by alternative splicing. Restricted expression patterns were observed for both *MYLK2* and *MYLK3*. *MYLK2* expression was only detected in skeletal muscle, whereas *MYLK3* expression was only observed in the heart (Figure 1E). *MYLK* was also found to be expressed in the heart, although its expression was not upregulated in failing myocardia as much as the expression of *MYLK3* (data not shown). To assess the physiological significance of cardiac-MLCK, we generated an adenovirus vector encoding cardiac-MLCK. In serum-free conditions, cultured neonatal rat cardiomyocytes showed predominantly disorganized sarcomere structures. Overexpression of cardiac-MLCK in cultured neonatal rat cardiomyocytes augmented sarcomere organization under serum-starved conditions (cells with organized sarcomeres, 28.7% ± 11.1% versus 3.1% ± 2.4%; $P < 0.001$; Figure 1, F and G), suggesting that cardiac-MLCK participates in sarcomere formation in cardiomyocytes.

Cardiac-specific myosin regulatory light chain is a specific substrate of cardiac-MLCK. Because this protein kinase contained a consensus kinase catalytic domain, we attempted to identify potential substrates of cardiac-MLCK. To identify physiological substrates of cardiac-MLCK, we screened murine heart homogenates using an in vitro kinase reaction. After fractionation of murine heart homogenates using a cation exchange column, aliquots of each fraction were subjected to an in vitro kinase reaction with recombinant cardiac-MLCK. Fractions 10 and 11 each contained a distinct 20-kDa band that was labeled with ^{32}P only in the presence of recombinant cardiac-MLCK (Figure 2A). This ^{32}P-labeled 20-kDa protein was purified (Figure 2B) and analyzed using matrix-assisted laser desorption/ionization-time-of-flight mass spectrometry and peptide mass fingerprinting. The 20-kDa protein contained fragments with amino acid sequences that were homologous to murine MLC2v (Figure 2C). No additional ^{32}P-labeled proteins were detected in fractions obtained following cation or anion exchange column purification. Further analysis of this phosphorylation event in vitro revealed endogenous MLC2v, purified from murine heart homogenates, was phosphorylated by recombinant cardiac-MLCK in a Ca^{2+}-calmodulin–dependent manner (Figure 2D). Thus, we conclude that cardiac-MLCK is a calmodulin-dependent kinase.

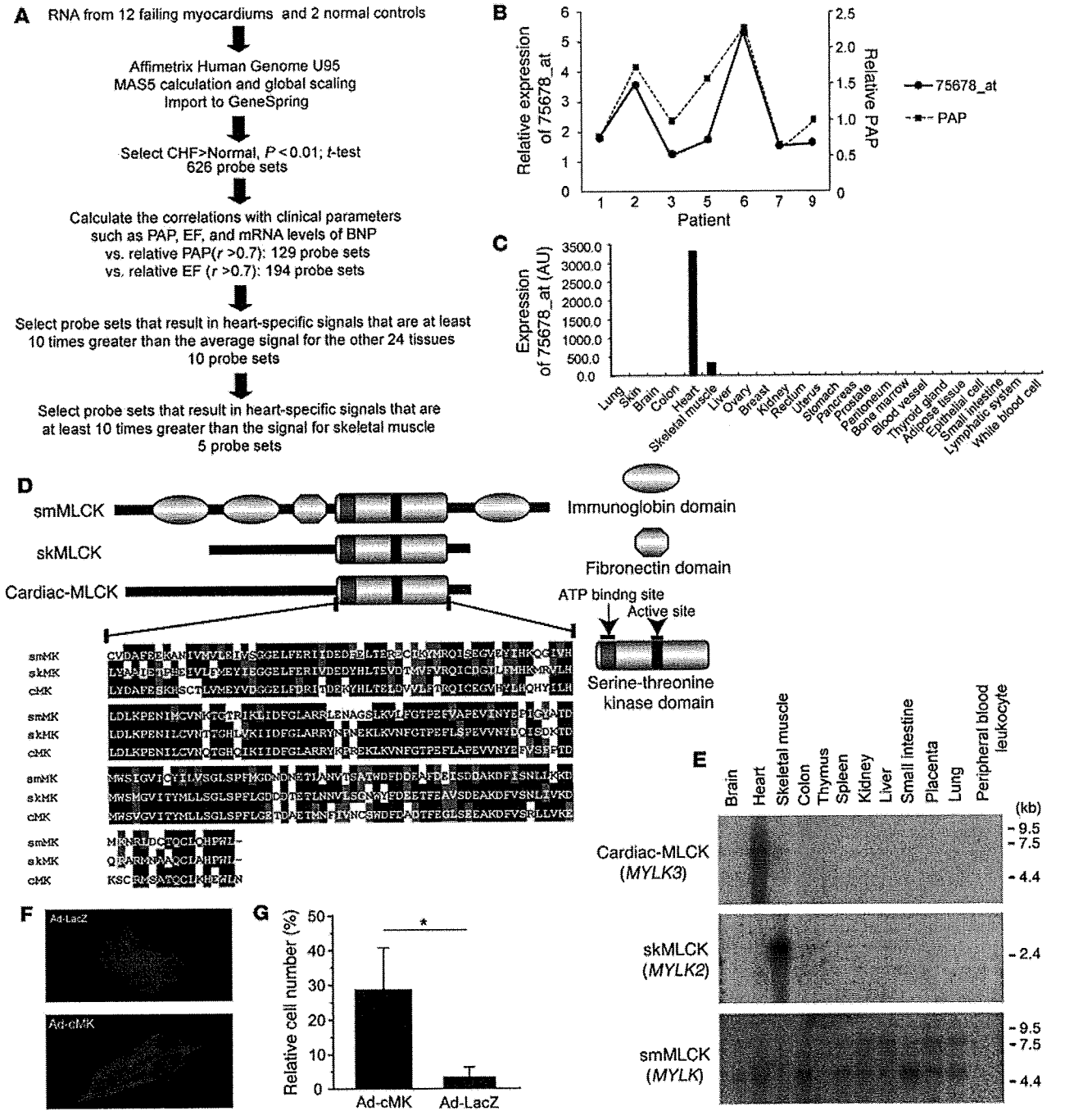

Figure 1

Microarray analysis for candidate gene selection. (**A**) Flowchart for the selection of candidate genes. (**B**) The relative expression levels of 75678_at correlated well with the relative PAP values in the respective patients. (**C**) Tissue localization of the candidate gene expression was analyzed using the GeneExpress database; 75678_at was specifically expressed in the heart. (**D**) Each MLCK family member possesses a highly conserved serine-threonine kinase domain in the C-terminal region of the protein. Amino acid residues on black backgrounds are the most commonly conserved residues at each position; residues on gray backgrounds are similar to the consensus amino acids. (**E**) Expression analysis of MLCK family members using multiple human tissue Northern blot membranes. The 2 transcripts transcribed from *MYLK* (encoding smMLCK) were ubiquitously expressed with the exception of skeletal muscle, thymus, and peripheral blood leukocytes. In contrast, *MYLK2* (encoding skMLCK) and *MYLK3* (encoding cardiac-MLCK) were only expressed in skeletal muscle and heart, respectively. (**F**) Fluorescence microscopy of cardiomyocytes cultured in serum-free conditions and infected with adenovirus encoding LacZ (Ad-LacZ) revealed predominantly round-shaped cells with disorganized sarcomere structures. Infection with adenovirus encoding cardiac-MLCK (Ad-cMK) at a MOI of 120 increased the number of the cells with organized sarcomere structures. Original magnification, ×1,000. (**G**) The percentage of cells with organized sarcomeres was significantly higher in cardiomyocytes infected with adenovirus encoding cardiac-MLCK than in those infected with adenovirus encoding LacZ. Values are mean ± SEM. *$P < 0.001$.

Next, we generated polyclonal antibodies specific for rodent cardiac-MLCK (RcMK). Antibodies that detected phosphorylated MLC2v (p-s15MLC; anti-rodent serine 15 phosphorylated MLC2v) and total MLC2v (tMLC) were also generated. RcMK detected rat cardiac-MLCK from whole-cell cardiomyocyte extracts as well as recombinant FLAG-tagged murine cardiac-MLCK (Figure 2E). Phosphorylated MLC2v and nonphosphorylated MLC2v could be clearly separated using urea-glycerol gel electrophoresis (12). tMLC detected both phosphorylated and nonphosphorylated MLC2v, whereas p-s15MLC specifically detected the phosphorylated form of MLC2v (Figure 2F). Overexpression of cardiac-MLCK increased the levels of phosphorylated MLC2v in cultured cardiomyocytes (Figure 2G). However, there was no effect on the expression of other sarcomere proteins involved in sarcomere organization such as troponin T, desmin, and α-actinin. mRNA expression of ANP and β myosin heavy chain, representative markers of cardiac hypertrophy, were also unaffected by cardiac-MLCK overexpression (data not shown). To further investigate the phosphorylation of MLC2v by endogenous cardiac-MLCK, we used specific siRNAs targeting cardiac-MLCK (si-cMKs). These siRNAs effectively suppressed the level of cardiac-MLCK mRNA by more than 70%, as determined using quantitative real-time PCR 24 hours after transfection (Figure 2H). These siRNAs also effectively suppressed the level of cardiac-MLCK protein and the amount of phosphorylated MLC2v 60–72 hours after transfection (Figure 2I), whereas no remarkable effects were seen for the expression of other sarcomere proteins. On the contrary, suppression of smMLCK expression, which is also distributed in heart, using siRNA targeting rat smMLCK (si-smMK) did not change either the phosphorylation status of MLC2v or the expression of sarcomere proteins (Figure 2J). These results indicated that cardiac-MLCK predominantly phosphorylates MLC2v, which is selectively expressed in cardiomyocytes. Thus, cardiac-MLCK may regulate morphologic change in cardiomyocytes, including sarcomere organization, through MLC2v phosphorylation.

Cardiac-MLCK regulates sarcomere assembly in cultured cardiomyocytes. To elucidate the precise role of cardiac-MLCK in the sarcomere structure, we analyzed the effects of MLC2v phosphorylation on sarcomeres in cultured neonatal rat cardiomyocytes. Polymerized actin stained with rhodamine-phalloidin revealed a regularly organized pattern of striations (Figure 3A). Phosphorylated MLC2v labeling with p-s15MLC demonstrated a similar striated pattern, although the labeling was predominantly observed in the A-band region, a portion of the sarcomere primarily made up of thick filaments (Figure 3, B–D). Diffuse cytosolic fluorescent labeling was seen when cardiac-MLCK was labeled with RcMK (Figure 3, E–G).

When cardiomyocytes were cultured in serum-free conditions, the organized striation pattern of actin was disrupted and the phosphorylated MLC2v-specific signal decreased (Figure 3K). To evaluate the morphologic changes observed in cardiomyocytes upon activation of endogenous cardiac-MLCK, we treated cardiomyocytes cultured under serum-free conditions with epinephrine. Stimulation of G protein–coupled receptors with epinephrine should activate cardiac-MLCK by increasing intracellular Ca^{2+} concentrations (13). A marked upregulation of MLC2v phosphorylation was obtained following treatment with 2 μM epinephrine (Figure 3H). Epinephrine-induced phosphorylation of MLC2v, which was observed as early as 5 minutes after stimulation, peaked within 30 minutes (Figure 3I). Treatment of the cardiomyocytes cultured in serum-free conditions with 2 μM epinephrine also induced reassembly of sarcomere structures and MLC2v phosphorylation (Figure 3, J, K, and L). To confirm the relevance of MLC2v phosphorylation by cardiac-MLCK, we introduced si-cMKs into cardiomyocytes and analyzed the sarcomere patterns in these cells. The level of phosphorylated MLC2v was reduced 72 hours after transfection with the si-cMKs; however, we did not observe any remarkable changes in the structures of the sarcomeres in cardiomyocytes cultured with serum. The sarcomeres of control siRNA– and si-cMK–treated cells contained organized filament structures (cells with organized sarcomeres, 97.0% ± 1.0% versus 90.0% ± 1.0%; NS; Figure 4, A–F and I). In contrast, the knockdown of cardiac-MLCK produced significant effects on sarcomere reassembly. si-cMK inhibited sarcomere reassembly after epinephrine treatment in cardiomyocytes cultured under serum-free conditions (cells with organized sarcomeres, 76.0% ± 8.5% versus 43.6% ± 7.0%; $P < 0.005$; Figure 4, A–F and I). We also confirmed the phosphorylation of MLC2v using immunoblot analysis (Figure 4G). The results of the immunoblot analysis are quantified in Figure 4H, and the relative MLC2v phosphorylation levels in this experiment exhibited a similar pattern as the percentages of cardiomyocytes with organized sarcomeres (Figure 4I), except in baseline, serum-containing conditions. These data suggest that MLC2v phosphorylation by cardiac-MLCK plays a critical role in initiating sarcomere reassembly.

Cardiac-MLCK is essential for normal cardiac development and function in zebrafish embryos. In order to further evaluate the physiologic roles of cardiac-MLCK, genetically engineered animals must be examined. In mice, however, targeted deletion of the cardiac ventricular myosin light chain, a specific substrate of cardiac-MLCK, was embryonic lethal at embryonic day 12.5 (6). Because cardiac-MLCK is an upstream modulator of MLC2v, deletion of the gene encoding cardiac-MLCK could also be embryonic lethal. Therefore, we performed in vivo knockdown experiments in *Danio rerio*, in which the phenotype generated by disrupting the functions of a targeted gene can be analyzed even if loss of the gene's functions is fatal. First, we generated a zebrafish cDNA library from which we cloned the zebrafish ortholog of *MYLK3* (*zmylk3*; encoding z-cardiac-MLCK). The amino acid sequence of cardiac-MLCK is highly similar to those of other vertebrate orthologs, especially within the C-terminal serine/threonine kinase domain (Figure 5A). Furthermore, like *MYLK3*, *zmylk3* is located between the genes VPS35 and NP001001436.1 (Assembly Zv5sc; Wellcome Trust Sanger Institute), indicating that this was the region of synteny between human and zebrafish. We also performed whole-mount in situ hybridizations using *zmylk3*-specific probes; the results indicated that *zmylk3* was expressed only in the heart at 24 and 48 hours postfertilization (hpf; Figure 5, B–I).

We injected zebrafish embryos with a specific MO directed against the AUG translational start site of the z-cardiac-MLCK mRNA (z-cMKaugMO). At 33 hpf, compared to control mock-injected zebrafish embryos, the heart region was slightly swollen in the z-cMKaugMO morphants. At 48 hpf, ventral swelling was observed in 45.6% ± 6.8% of the z-cMKaugMO morphants (Figure 6A). The ventral swelling became more apparent at 72 hpf (Figure 6B). In contrast, zebrafish embryos injected with an MO containing 5-base mismatches compared with z-cMKaugMO were indistinguishable from control zebrafish embryos (Figure 6C). We further examined the effects of 3 additional MOs, which were targeted to delete specific exons of z-cardiac-MLCK and z-MLC2v. Of these MOs, 2 were directed against the splice donor and acceptor

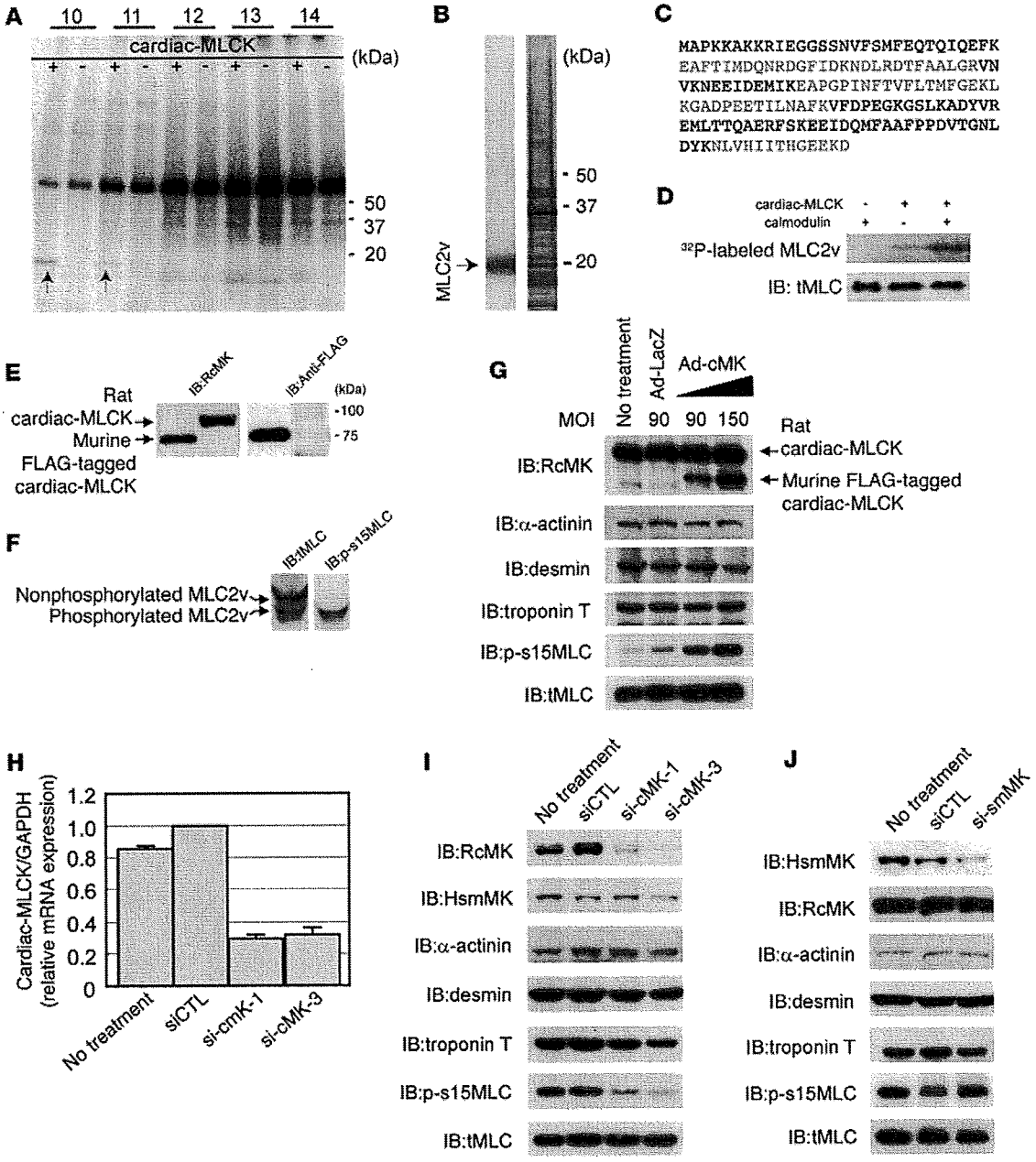

Figure 2

Identification of MLC2v as a specific substrate of cardiac-MLCK. (**A**) A putative 20-kDa substrate that was labeled with P^{32} in the presence of cardiac-MLCK was identified in fractionated murine myocardium extracts (arrows). Fraction numbers are shown at top. (**B**) P^{32}-labeled MLC2v was purified and visualized by autoradiography (left lane) and silver staining (right lane). (**C**) Peptides from the purified protein, which matched the sequences of murine MLC2v, are shown in red. (**D**) Purified MLC2v from murine myocardia was phosphorylated by cardiac-MLCK in a Ca^{2+}-calmodulin–dependent manner. (**E**) RcMK detected rat cardiac-MLCK from cultured cardiomyocyte cell extracts and FLAG-tagged murine cardiac-MLCK. (**F**) Nonphosphorylated MLC2v and phosphorylated MLC2v were separated using urea-glycerol gel electrophoresis. tMLC and p-s15MLC were confirmed to specifically detect each target protein. (**G**) Overexpression of murine cardiac-MLCK in cultured cardiomyocytes following infection with an adenovirus vector encoding murine cardiac-MLCK at MOIs of 90 and 150 upregulated the phosphorylation of MLC2v in a dose-dependent manner. Endogenous rat cardiac-MLCK is shown at top; overexpressed murine cardiac-MLCK is shown below. (**H** and **I**) Both si-cMK-1 and si-cMK-3 effectively suppressed the mRNA (**H**) and protein levels (**I**) of cardiac-MLCK, resulting in reduced phosphorylation of MLC2v. smMLCK, α-actinin, desmin, and troponin T were not affected by suppression of cardiac-MLCK expression. siCTL, control siRNA. (**J**) The protein levels of smMLCK were effectively decreased by si-smMK; no remarkable changes were observed in protein levels of phosphorylated MLC2v or other sarcomere-related proteins.

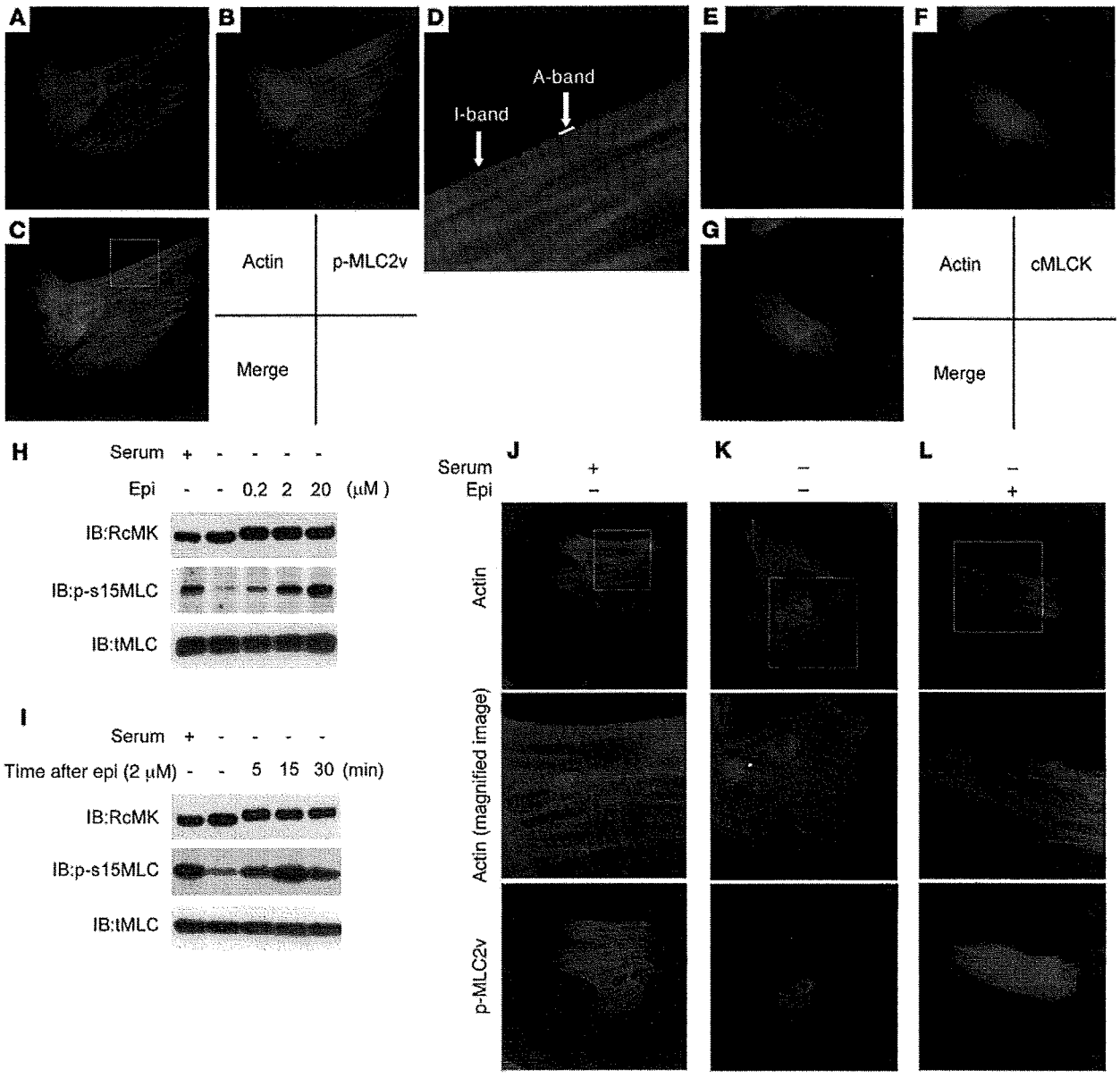

Figure 3

Epinephrine treatment induced sarcomere assembly through MLC2v phosphorylation. Original magnification, ×1,000 (**A–C** and **E–G**). (**A–D**) Polymerized actin stained with rhodamine-phalloidin (**A**) as well as phosphorylated MLC2v labeled with p-s15MLC (**B**) exhibited regular patterns of striation. (**C**) Merged image of **A** and **B**. (**D**) Higher magnification of boxed area in **C** revealed that rhodamine-phalloidin predominantly stained the I-band, whereas phosphorylated MLC2v (p-MLC2v) was localized in the A-band. Original magnification, ×4,000 (**D**). (**E–G**) Cardiac-MLCK (cMLCK) labeled with RcMK showed a diffuse cytosolic labeling pattern. (**H**) Cultured cardiomyocytes were stimulated with 0.2–20 μM epinephrine (Epi), which upregulated MLC2v phosphorylation in a dose-dependent manner. (**I**) Cultured cardiomyocytes were stimulated with 2 μM epinephrine for the indicated time periods. Epinephrine-induced phosphorylation of MLC2v in cultured cardiomyocytes was observed as early as 5 minutes after stimulation; maximal phosphorylation was obtained after approximately 30 minutes. (**J–L**) Cardiomyocytes cultured with serum contained organized patterns of striation and a moderate level of MLC2v phosphorylation. Middle panels show higher magnification of boxed regions in top panels. Cardiomyocytes cultured in serum-free conditions were incubated in the absence (**K**) or presence (**L**) of 2 μM epinephrine. (**K**) Cardiomyocytes cultured under serum-free conditions contained disorganized, punctuated actin staining with a reduced level of MLC2v phosphorylation. (**L**) Stimulation with epinephrine provoked rapid sarcomere reassembly and augmented MLC2v phosphorylation. Original magnification, ×1,000 (**J–L**, upper and lower panels); ×3,000 (**J–L**, middle panels).

sites of exons 4 and 6 of z-cardiac-MLCK, respectively. Deletion of exon 4 caused a frameshift and resulted in premature termination of the transcript. Exon 6 includes the catalytic center of z-cardiac-MLCK, and its deletion was expected to diminish the protein's kinase activity. The third MO was designed to delete exon 2 of z-MLC2v, which includes the phosphorylatable serine. These 3

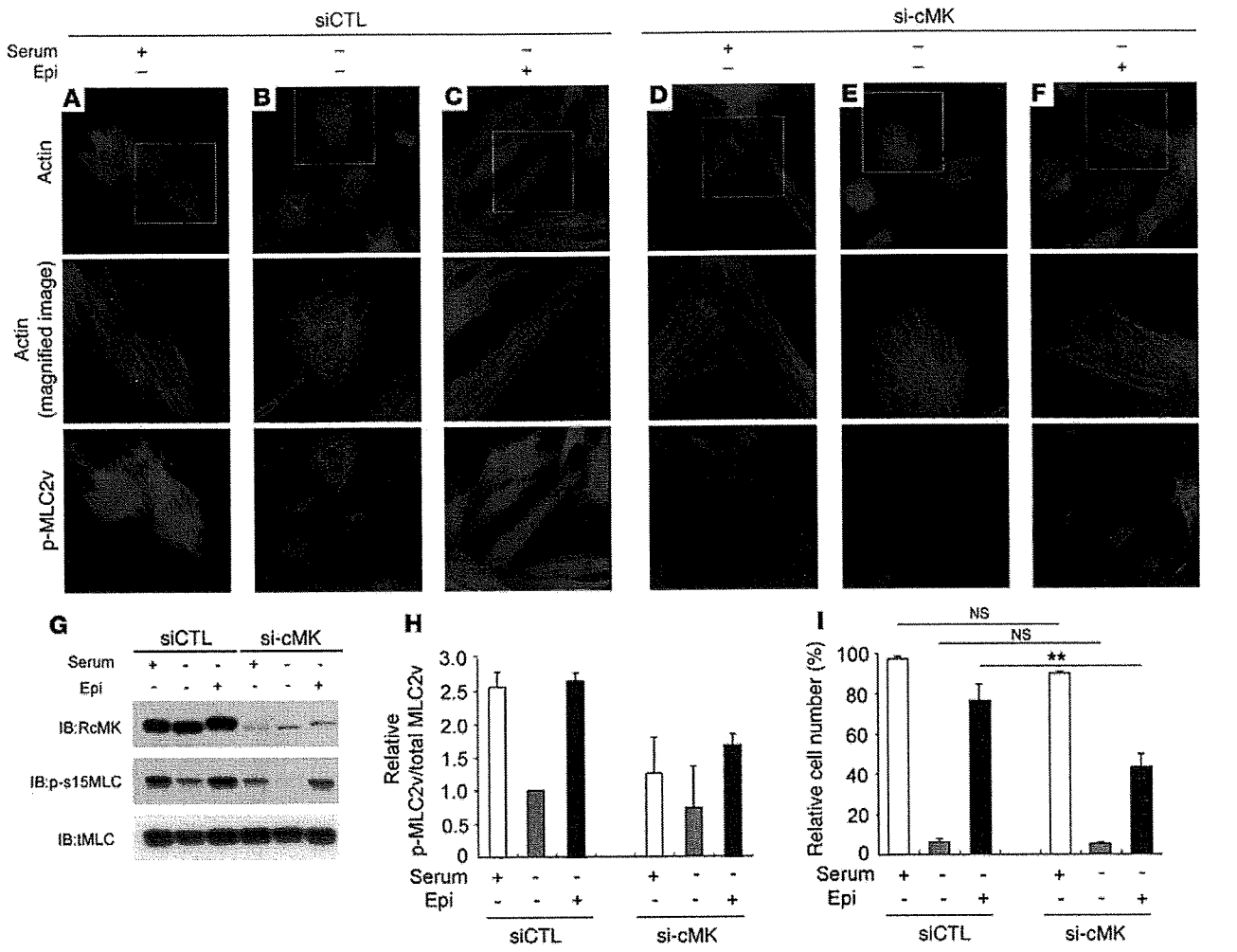

Figure 4

Cardiac-MLCK regulates the initiation of sarcomere assembly in cultured cardiomyocytes through MLC2v phosphorylation. Original magnification, ×1,000 (upper and lower panels); ×2,000 (middle panels). (**A–F**) Cardiomyocytes were transfected with control siRNA (**A–C**) or si-cMK (**D–F**). Middle panels show higher magnification of boxed regions in top panels. In serum-containing conditions, si-cMK–transfected cardiomyocytes showed reduced levels of MLC2v phosphorylation (**D**) compared with control siRNA–transfected cardiomyocytes (**A**), although both exhibited regularly organized sarcomere structures. Actin staining in cardiomyocytes cultured in serum-free conditions revealed a punctuated pattern in the sarcomeres (**B** and **E**); moreover, the degree of MLC2v phosphorylation was reduced in the si-cMK–transfected cardiomyocytes compared with the control siRNA–transfected cardiomyocytes. Stimulation with 2 μM epinephrine provoked upregulation of MLC2v phosphorylation and sarcomere reassembly in control siRNA–transfected cardiomyocytes (**C**), but not in si-cMK–transfected cardiomyocytes (**F**). (**G**) We confirmed the levels of MLC2v phosphorylation shown in **A–F** using immunoblot analysis. (**H**) Quantitation of the levels of phosphorylated MLC2v shown in **G**. Values are mean ± SEM. (**I**) Percentage of the cells with organized sarcomeres. There was no significant difference between the populations of cardiomyocytes transfected with control siRNA and si-cMK under either serum-containing or serum-free conditions. The percentage of the cells with organized sarcomeres was significantly higher for the control siRNA–transfected cardiomyocytes than for the si-cMK–transfected cardiomyocytes. Values are mean ± SEM. p-MLC2v, phosphorylated MLC2v. $^{**}P < 0.001$.

MOs effectively deleted the targeted exons, inducing comparable ventral swelling phenotypes (Figure 6, D–F). The finding that 4 different MOs produced similar results suggests that the cardiac phenotypes resulted from a loss of the kinase activity of z-cardiac-MLCK. To evaluate the cardiac phenotype of the z-cMKaugMO morphants in detail, we examined the SAG4A zebrafish strain, which specifically expresses GFP in the cardiac ventricle (14). After injecting z-cMKaugMO into SAG4A embryos, cardiac motion at 72 hpf was imaged with a high-sensitivity digital camera attached to a fluorescence stereomicroscope (Figure 6G and Supplemental Movies 1 and 2; supplemental material available online with this article; doi:10.1172/JCI30804DS1). Recordings were converted to motion mode (M-mode) images using our original software (Figure 6H). From these images, we determined the end-diastolic dimension (Dd), end-systolic dimension (Ds), and fractional shortening (FS) of the cardiac ventricle. These data are summarized in Table 2, and the results indicate that the cardiac dimensions of the z-cMKaugMO morphants were significantly larger than those of control zebrafish embryos (Dd, 79.6 ± 3.7 versus 117.0 ± 10.4 μm; Ds, 50.3 ± 6.5 versus 76.0 ± 7.0 μm; $P < 0.0001$ for both com-